Structural Alterations of Upper Cervical Spinal Cord in Ataxic and Non-ataxic Mutation Carriers of Spinocerebellar Ataxia Type 3 (SCA3)

Inaugural-Dissertation

zur Erlangung des Doktorgrades

der Hohen Medizinischen Fakultät

der Rheinischen Friedrich-Wilhelms-Universität

Bonn

Berkan Serdal Can Koyak

aus Bursa/Türkei

2022

Angefertigt mit der Genehmigung
der Medizinischen Fakultät der Universität Bonn

1. Gutachter: Prof. Dr. Thomas Klockgether

2. Gutachter: PD Dr. Daniel Loyd Robert Kütting

Tag der Mündlichen Prüfung: 21.07.2022

Aus der Klinik und Poliklinik für Neurologie
Direktor: Prof. Dr. med. Thomas Klockgether

I dedicate this dissertation to lucky coincidences.

Table of contents

	List of abbreviations	7
1.	**Introduction**	11
1.1	Epidemiology	11
1.2	Genetics	11
1.3	Pathophysiology	15
1.4	Clinical Features	16
1.4.1	SCA3	17
1.5	Diagnosis	18
1.6	Background	19
1.6.1	Neuroanatomical Involvement	19
1.6.2	Treatment	20
1.6.3	Early Changes	21
1.6.4	MRI as a Biomarker	21
1.6.5	Objective	23
2.	**Materials and methods**	24
2.1	General Characteristics of the Cohort	24
2.2	Participants	24
2.3	Clinical Scale	25
2.4	Group Definition	25
2.5	Imaging Acquisition	25
2.6	Cervical Spinal Cord Volumetry	26
2.7	Manual Delineation	26
2.8	Semi-automated Segmentation	27
2.9	Statistical Analysis	30
3.	**Results**	31
4.	**Discussion**	44
5.	**Summary**	48
5.1	Objective	48
5.2	Methods	48

5.3 Results 48
5.4 Conclusion 48
6. List of figures 49
7. List of tables 50
8. References 51
9. Acknowledgement 57
10. Publications 58

List of abbreviations

ADCA	Autosomal dominant cerebellar ataxias
ALS	Amyotrophic lateral sclerosis
ANCOVA	Analysis of Covariates
ANOVA	Analysis of Variance
AP	Anteroposterior(midsagittal) diameter
ATXN	Ataxin
CCFS	Composite Cerebellar Functional Severity
CI	Confidence Interval
CSA	Cross-sectional area
CSF	Cerebrospinal fluid
DMD	Duchenne muscular dystrophy
DRPLA	Dentatorubro-pallidoluysian atrophy
DTI	Diffusion tensor imaging
DUB	Deubiquitinase
EUROSCA	European integrated project on spinocerebellar ataxias
FDA	Food and Drug Administration
Fig	Figure
fMRI	Functional MRI

GM	Grey Matter
HD	Huntington’s disease
IQR	Interquartile range
LR	Left to right(midcoronal) diameter
MJD	Machado-Joseph disease
MRI	Magnetic resonance imaging
MRS	Magnetic resonance spectroscopy
MS	Multiple Sclerosis
NAA	N- acetylaspartate
NES	Nuclear export sites
NESSCA	Neurological Examination Score for Spinocerebellar Ataxia
NfL	Neurofilament light
NLS	Nuclear-localization signal
PET	Positron emission tomography
Pol II	Polymerase II
polyA	Polyalanin
polyQ	Polyglutamine
polyS	Polyserine
RAN	Repeat associated non-ATG translation

RBP	RNA binding protein
REM	Rapid eye movement
RISCA	Prospective study of individuals at risk for SCA1, SCA2, SCA3 and SCA6
ROI	Region of interest
SARA	Scale for the assessment and rating of ataxia
SCA	Spinocerebellar ataxia
SCAFI	SCA Functional Index
SCT	Spinal Cord Toolbox
SD	Standard deviation
SE	Standard error
SMA	Spinal muscular atrophy
T	Tesla
Tab	Table
TBP	TATA-binding protein
Ub	Ubiquitin
UIMs	Ub-interacting motifs
UTR	Untranslated region
VBM	Voxel-based morphometry

WES	Whole-exome sequencing
WGS	Whole-genome sequencing
WM	White Matter

1. Introduction

Spinocerebellar ataxias (SCA) are a group of autosomal dominantly inherited genetic diseases, primarily characterized by progressive cerebellar ataxia resulting in loss of balance and coordination accompanied by slurred speech and oculomotor abnormalities. Most SCAs present with additional non-ataxia symptoms. SCAs are named with a number, which represents the chronological discovery of the underlying disease mutation. Firstly, I would like to outline the genetics, clinical features and therapeutic options of SCAs with a focus on SCA3.

1.1 Epidemiology

Epidemiological data for SCAs are markedly varying from country to country **(Fig. 1)**. In a systematic review from Ruano et. al, in which 22 epidemiological studies from 16 countries were included, the prevalence of SCAs ranged between 0.0–5.6/100.000 with an average of 2.7/100.000 (95 % CI: 1.5 – 4.0/100.000). SCA3 or Machado-Joseph disease (MJD) was found to be the most frequent subtype, followed by SCA2 and SCA6 (Ruano et al., 2014). However, in isolated geographical areas, much higher prevalence rates were reported, as on the Azores Islands, with the highest prevalence of 1/239 on Flores Island (Coutinho et al., 2013). This discrepancy might be explained by the founder effect, which appears either through the migration of individuals carrying mutation or de novo mutations. According to a review study of Bettencourt and Lima, SCA3 is especially prevalent in Brazil (counting for 69–92 % of all SCA families), China (48−49 %), the Netherlands (44 %), Germany (42 %) and Japan (28–63 %). On the contrary, it is less frequent in the USA and Canada (21–24 % of SCA families), France (20 %), Mexico (12 %), Australia (12 %) and India (5–14 %), South Africa (4 %) and Italy (1 %) (Bettencourt and Lima, 2011).

1.2 Genetics

Up to now, more than 45 subtypes of SCAs were defined, which are either caused by repeat expansions or conventional non-repeat mutations. Repeat expansion mutations can be further divided into polyglutamine(polyQ)-coding CAG repeat expansions and

non-protein coding repeat expansions. **(Fig. 2)** CAG repeats result in an elongated polyQ portion in the affected disease protein, which is the common feature of polyQ disorders. SCA1, SCA2, SCA3 and SCA6 have polyQ repeats as the underlying genetic cause and they are the most prevalent subtypes, which together take up more than 50 % of all SCA genotypes. Spinal and bulbar muscular atrophy (SBMA) and Huntington's disease (HD) are other examples of polyQ diseases. **(Fig. 3)** The CAG repeat length of the expanded allele is associated with early disease onset and disease severity (Jacobi et al., 2015).

Repeat expansions are unstable. During transmission to next generations, the repeat number can increase, resulting in earlier disease onset and more severe phenotype. This phenomenon is called anticipation, which is a common feature of repeat expansion disorders.

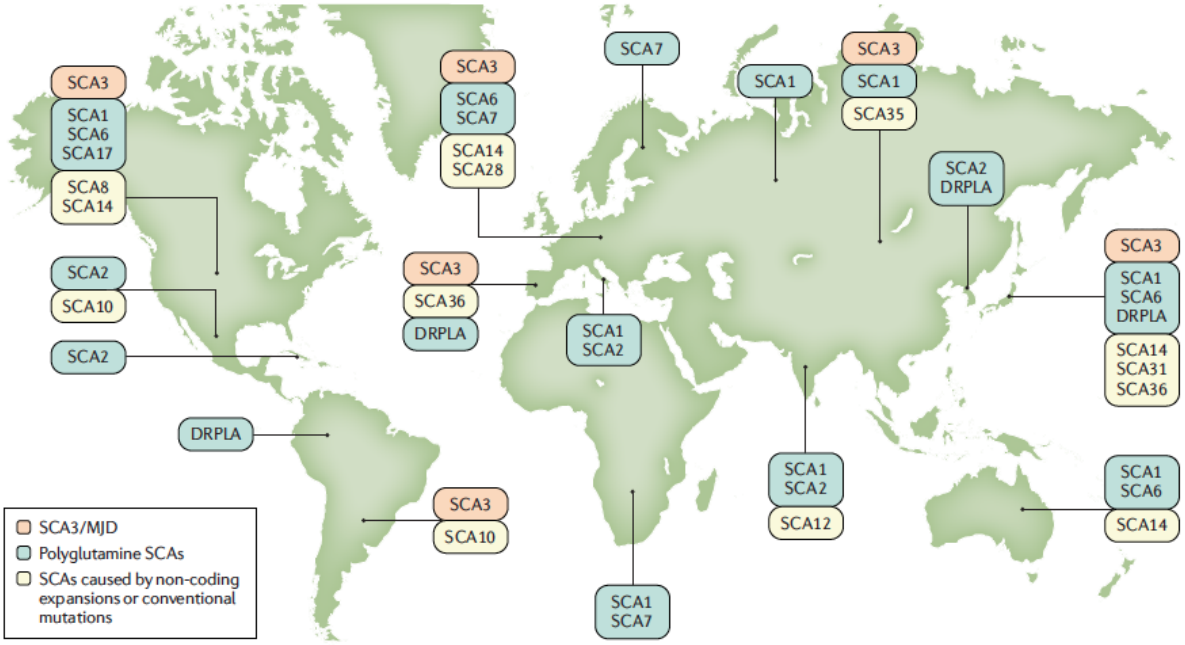

Fig.1: Epidemiological distribution of SCAs(modified from Klockgether et al., 2019)
The most frequent SCA subtypes vary by countries considerably, represented by three groups which can be extracted from the legend on the left below.

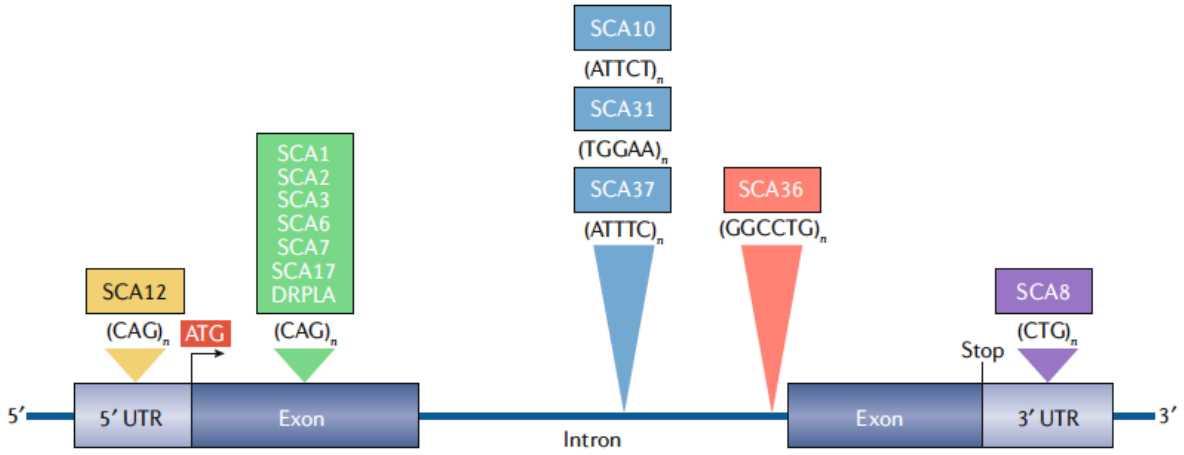

Fig. 2: Coding and non-coding repeat expansion SCAs (modified from Ashizawa et al., 2018) This illustration shows the affected region of DNA for different repeat expansion SCAs green: polyQ SCAs, ATG: start codon, UTR: untranslated region

Tezenas et al. proposed a model to estimate the age of onset in non-ataxic mutation carriers in European cohorts (Tezenas du Montcel et al., 2014). The calculation is based on the repeat length of the longer allele and the actual age. However, geographical origin is found to play a key role in explaining the variability of disease onset. In a population study with 739 SCA3/MJD carriers from South Brazil, Taiwan and the Portuguese Azorean islands, Mattos et al., 2019 suggested that this formula underestimated the observed age of onset in South Brazilian and Taiwanese test cohorts. Furthermore, in a meta-analysis of 10 individual-participants (n=2099) and 2 aggregated data cohorts with SCA3 mutation carriers, geographical origin alone was responsible for 8.3 % variance of age of onset. CAG length of the longer ATXN3 allele explained 55.2 % of variance alone, whereas it was 73.5 % when geographical origin, family effects and CAG repeats of ATXN2 alleles were included in the linear regression model (de Mattos et al., 2018).

SCA3 is caused by a prolonged CAG repeat in the ATXN3 gene (14q32.1), which translates to the mutation protein called ataxin3. **(Fig. 4)** Ataxin3 is accumulated in intranuclear inclusions of affected neurons (Paulson et al., 1997).

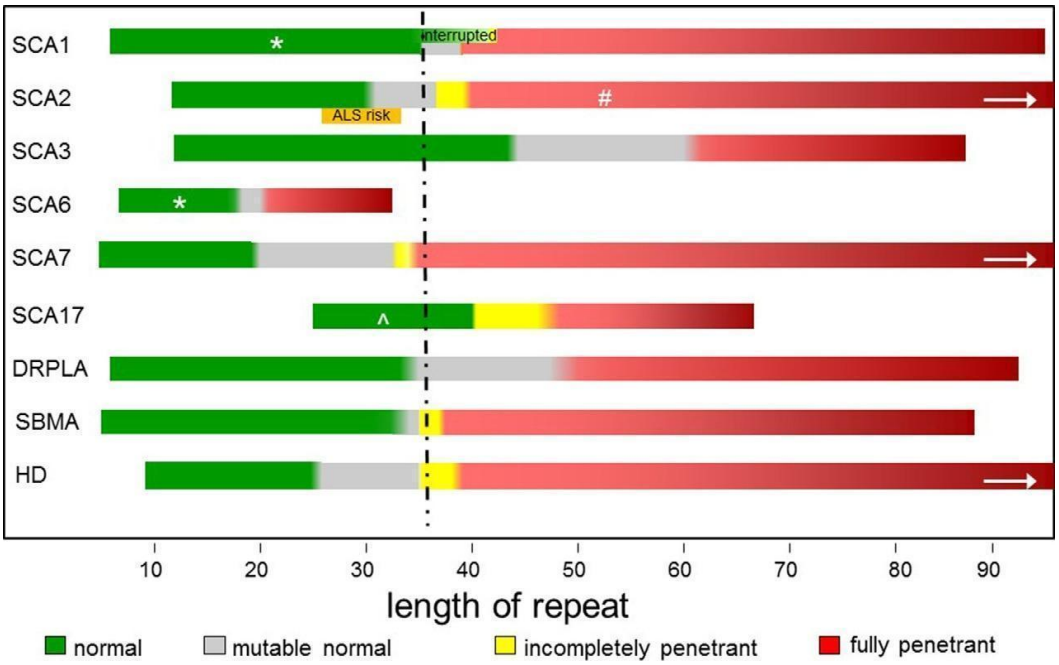

Fig. 3: Normal and disease repeat lengths for the CAG/polyglutamine diseases (modified from Paulson, 2018)

Color coded scheme for the CAG/polyglutamine diseases SCA1, SCA2, SCA3, SCA6, SCA7, SCA1, dentatorubral-pallidoluysian atrophy (DRPLA), spinal and bulbar muscular atrophy (SBMA) and Huntington's disease (HD). Normal (green), incompletely penetrant (yellow), and fully penetrant (red) repeat lengths are shown for each disease. Deepening color of red illustrates increased disease severity and earlier age of onset related to longer repeat lengths. Arrows illustrate that the longest disease repeats in SCA2, SCA7 and HD are > 100 repeats. Gray regions represent a size range of intermediate-length repeats that may be prone to further expansion. High normal SCA2 alleles (orange) are a risk factor for amyotrophic lateral sclerosis (ALS). At SCA1 locus, normal repeats can be longer when they are interrupted by cytosine adenine thymine (CAT) residues.

* Normal repeat lengths in SCA1 and SCA6 are modifiers of age of onset, and SCA6 normal repeat length is also a modifier of age of onset in SCA2.

In SCA2 disease repeats interrupted by CAA can be associated with dominantly inherited Parkinson disease rather than ataxia.

^ Normal repeat length in SCA17 is an imperfect CAG repeat interrupted with CAA residues.

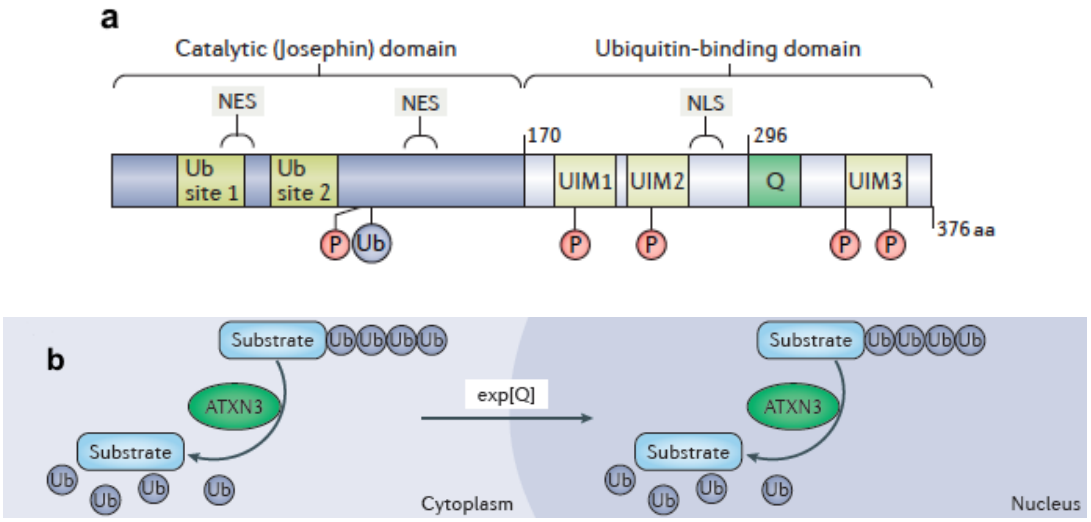

Fig. 4: Molecular structure and function of ATXN3 (modified from Paulson et al., 2017)

a. The deubiquitinase (DUB) ATXN3 has an N-terminal catalytic (Josephin) domain, which contains two Ubiquitin-binding sites and two nuclear export sites (NES), and a C-terminal Ubiquitin-binding domain bearing three Ubiquitin-interacting motifs (UIMs) and a nuclear-localization signal (NLS).

b. ATXN3 binds and cleaves polyubiquitin chains and has been implicated in a variety of ubiquitin (Ub)-dependent protein quality control pathways. Although expanded ATXN3 retains DUB activity in vitro, changes in polyQ-repeat length may alter its function in the complex cellular environment, with deleterious consequences. As with many polyQ disease proteins, mutant ATXN3 becomes concentrated in the nucleus.

NLS: nuclear-localization signal

1.3 Pathophysiology

In SCAs, mainly Purkinje fibers of the cerebellum degenerate. However, with emerging neurological diagnostic modalities, the involvement of spinal cord, brain stem, dentate nucleus, basal ganglia, peripheral and autonomic nervous system and in advanced stages cerebral cortex and subcortical white matter (WM) were demonstrated as well (Rezende et al., 2018; Scherzed et al., 2012).

Protein toxicity plays a fundamental role in pathogenesis. It is shown that not only the mutation protein itself but also the interacting proteins showed an altered function, which amplifies the extent of toxicity. Mutation proteins are prone to oligomerization and aggregation, which tends to be restricted to intracellular if not intranuclear space

because of the fact that, all disease proteins reside intracellularly except ATXN6, which is a transmembrane subunit of a calcium channel. Intranuclear inclusions include fragments of disease proteins and are detected in affected brain regions. Their mere presence might impair the nuclear integrity by interfering processes such as transcription, splicing or even gene expression (Paulson et al., 1997).

Apart from protein mediated mechanisms, RNA toxicity and repeat associated non-ATG translation (RAN) are examples of RNA mediated pathogenesis. **(Fig. 5)** Ion channelopathy, mitochondriopathy and protein phosphorylation (e.g serine 776 phosphorylation on ATXN1 gene) were put forward as well.

1.4 Clinical Features

Spinocerebellar ataxias differ in their clinical presentation not only between genotypes but also within genotypes. Even though it is less used nowadays, Harding's classification is still useful to get a first insight about clinical phenotypes. According to that classification, there are three main groups for autosomal dominant cerebellar ataxias (ADCA): In ADCA1, ataxia is accompanied by non-ataxia signs, with e.g. SCA1, SCA2 and SCA3 (MJD) falling into that category. ADCA3 stands for pure cerebellar disorders, where SCA6 is probably the most prominent example for that category. ADCA2 represents a quite rare combination of ataxia accompanied by progressive visual loss due to retinal degeneration as e.g. in SCA7 (Harding et al., 1983).

Nevertheless, progressive loss of balance and coordination accompanied by slurred speech with an onset in adult life are common symptoms of most of the SCAs. Gait ataxia is often the first manifestation, which attracts the patients´ attention. As disease progresses; coordination deficits of the upper limbs may appear, presenting with clumsiness, writing difficulties and loss of fine-motor skills. Oculomotor abnormalities can present in a wide spectrum, including broken-up smooth pursuit, gaze-evoked nystagmus, gaze paresis, dysmetric saccades, saccade slowing, diplopia, reduced optokinetic nystagmus and impaired visual suppression of the vestibulo-ocular reflex. Non-ataxia symptoms such as spasticity, rigidity, dystonia, myoclonus, retinopathy, optic

atrophy, peripheral neuropathy and cognitive impairment may also be present. In addition, restless leg syndrome, REM sleep behaviour disorder and depression are common comorbidities. In the course of the disease, physical disability deteriorates which makes the use of a wheelchair inevitable (Klockgether, 2008).

In the European integrated project on spinocerebellar ataxias (EUROSCA) study with a median observational time of 49 months, disease progression, measured by Scale for the assessment and rating of ataxia (SARA), was fastest in SCA1, intermediate in SCA2 and SCA3 and slowest in SCA6. The annual SARA score increase in the SCA3 group was 1.56 points (Jacobi et al., 2015). The mean age of onset was the 3rd or 4th decade of life in SCA1, SCA2 and SCA3; and roughly two decades later in SCA6 (Warrenburg et al., 2005).

1.4.1 SCA3

SCA3 is the most common autosomal dominant ataxia worldwide (Fahl et al., 2015). A synonym is Machado Joseph disease (MJD). Four different subtypes have been defined: early-onset disease with large CAG expansions, extrapyramidal signs, spasticity and minimal ataxia (Type 1); midlife progressive ataxia with upper motor neuron signs as most common form (Type 2); late-onset ataxia with short CAG expansions, peripheral neuropathy, subsequent amyotrophy and hyporeflexia (Type 3); and parkinsonism with or without ataxia (Type 4), but there is wide overlap between these types, so that this classification is of limited relevance (Fahl et al., 2015, Paulson et al., 2012). Ataxia of gait, stance and limb movements, dysarthria, sensory disturbances, pyramidal signs, dystonia, ophthalmoplegia, bulging eyes, peripheral neuropathy, sleep disturbances and restless legs syndrome are common accompanying symptoms (Klockgether, 2008; Schöls et al., 2004). SCA3 is finally leading to premature deaths (Mendonça et al., 2018).

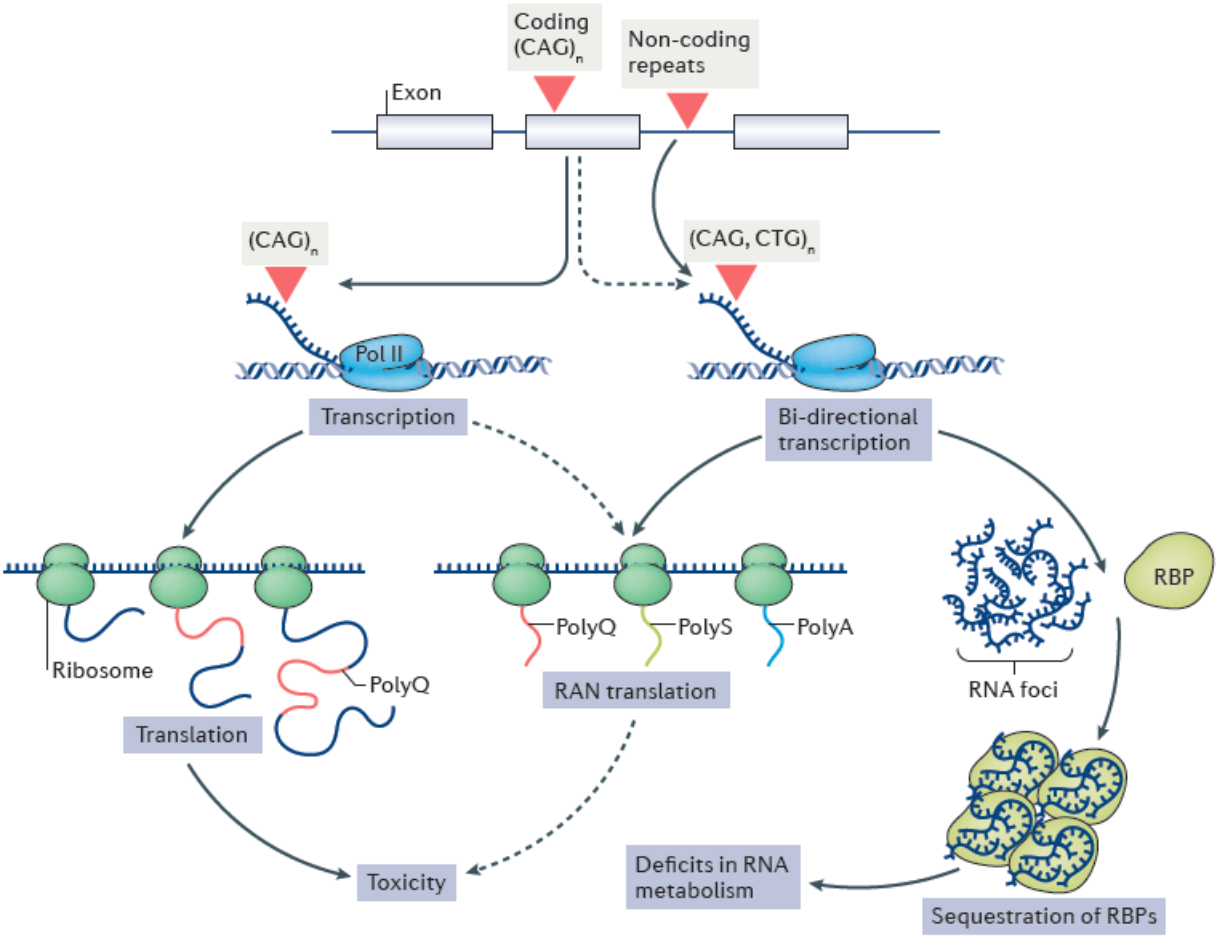

Fig. 5: RNA toxicity and RAN translation (modified from Paulson et al., 2017)

RAN is an aberrant bidirectional translation mechanism, encoding polyserine and polyalanine apart from polyglutamine in the absence of an ATG start codon, raising the possibility that these homopolymeric proteins are toxic as well. It is first evidenced in vitro in SCA8, but might be applicable to polyQ disorders (Zu et al., 2011).

polyQ: polyglutamine, polyS: polyserine, polyA: polyalanine, Pol II: polymerase II RBP: RNA binding protein

1.5 Diagnosis

Diagnosing hereditary ataxias is a challenging task, which necessitates the elimination of non-hereditary causes at first. Family history, if informative, might be helpful. However, a negative family history does not rule out SCAs (Klockgether, 2010). Death of parents before disease onset, as it may occur in SCA6, which appears relatively late in

the 6th decade of life, may mask a positive family history. Novel or de novo mutations can also occur. Friedreich's Ataxia should be taken into consideration as the most common recessive ataxia, which is a repeat expansion disease and can easily be tested (Ashizawa et al., 2018).

In SCAs, phenotype alone does not allow to predict the genotype, except SCA7 presenting with visual loss. For that reason, diagnosis can only be made by genetic tests targeting the relevant disease mutation loci. If suspected, SCA1, SCA2, SCA3 and SCA6 should be tested first owing to their high prevalence, unless there is a known mutation in family members or the patient comes from a high prevalent region (Klockgether et al., 2019). These high prevalence mutations are not detected by whole-exome sequencing (WES), which should therefore not be used as the first line diagnostic tool. WES should rather be used, after repeat mutations have been negatively tested.

1.6 Background

1.6.1 Neuroanatomical Involvement

The atrophy of cerebellum, brainstem, basal ganglia and cerebral cortex has been shown in magnetic resonance imaging (MRI) studies comparing symptomatic SCA3 mutation carriers and healthy controls (Bürk et al, 1996; Klockgether, 1998; Wüllner et al, 1993). However, pathoanatomical studies with SCA3 revealed an even more extensive damage (Rüb et al., 2008). In a recent cross-sectional MRI study, investigating the structural alterations in SCA3 mutation carriers over the whole time course of the disease including the presymptomatic phase, a caudo-rostral disease progression pattern is hypothesized, which can roughly be summarized as involvement of spinal cord, cerebellar peduncles and substantia nigra in the beginning, followed by brainstem and basal ganglia diffusely, and cerebral cortex in advanced stages (Rezende et al, 2018).

1.6.2 Treatment

Currently, there is no approved medication available for any SCA. Only supportive therapies such as coordinative physiotherapy, occupational therapy and speech therapy are available and of limited benefit on halting disease progression and preserving mobility (Chang et al., 2015; Ilg et al., 2009).

Therapeutic medication like 4-aminopyridine, chlorzoxazone, riluzole, valproic acid, varenicline and lithium carbonate are examples of potential drug candidates in SCAs (Ashizawa et al., 2018). Up to now, no significant therapy effect on symptoms or disease progression could be shown. Disease modifying therapies studied in SCA3 animal or cell models include dantrolene, citalopram, aripiprazole and novel gene-silencing methods (e.g. small interfering RNA (siRNA), micro RNA(miRNA) or antisense oligonucleotides (ASO)) (Alves et al., 2008; Ashraf et al., 2018; do Carmo Costa et al., 2013; Chen et al., 2008; Costa et al., 2016; Moore et al., 2017). Targeting the disease causing mechanisms directly on the gene level including transcription or translation is of special interest for future interventional trials. These are already in use for other hereditary neurological disorders. Especially the approval of eteplirsen and nusinersen for Duchenne muscular dystrophy (DMD) and spinal muscular atrophy (SMA) by the Food and Drug Administration (FDA) were encouraging. Furthermore in another polyQ disorder, Huntington's disease(HD), the administration of an ASO-based agent in a phase I/IIa trial with early stage patients resulted in decreased cerebrospinal fluid (CSF) levels of huntingtin (Tabrizi et al., 2019).

For future clinical trials, early detection and intervention is of crucial importance. In a study with SCA1 mutation carrier transgenic mice, knockout of ATXN1 gene at an earlier stage resulted in complete recovery presented with improvement of motor symptoms and even clearance of nuclear inclusions from Purkinje fibers. In later disease stages, the therapy response was much weaker (Zu et al., 2004). Therefore, in the presymptomatic disease phase, where clinical scales are lacking sensitivity there is an urgent need for blood, CSF or imaging biomarkers to describe and detect disease related alterations.

1.6.3 Early Changes

Disease onset is usually defined by the first appearance of gait disturbances. Some groups define disease onset by the appearance of any first disease related symptom, including e.g. handwriting problems or double vision. The European multicentre RISCA study with 276 non-ataxic first-degree relatives of SCA1, SCA2, SCA3 and SCA6 patients from 178 families revealed some early changes preceding ataxia. Voxel-based morphometry showed grey matter loss in medulla oblongata and pons of presymptomatic SCA1 mutation carriers. Brainstem volumes were reduced in presymptomatic SCA2 mutation carriers. Subjects closer to the estimated age of onset had higher SARA scores in SCA1 and SCA2. In several coordination tests, the non-carrier relatives performed better than presymptomatic SCA1 and SCA2 mutation carriers. Horizontal gaze evoked nystagmus had a significantly higher prevalence in non-ataxic SCA3 mutation carriers (Jacobi et al., 2013). In the follow-up study of the above-mentioned cohort; hyperreflexia in SCA1, broken-up smooth pursuit in SCA3 and nystagmus in SCA3 occurred before ataxia onset. Double vision was the strongest predictor of conversion to ataxia in SCA3 (Jacobi et al., 2020).

So, to sum up, the pre-ataxia stage may present with mild coordination deficits, oculomotor symptoms, neurodegeneration with atrophy of brainstem structures as well as cerebellum.

As mentioned above, the early changes, especially in the pre-ataxic stage of the disease are crucial, since they will play a central role as potential biomarkers in the anticipated treatment window for gene modifying treatments.

1.6.4 MRI as a Biomarker

The National Institutes of Health Biomarkers Definitions Working Group defines a biomarker as “a characteristic, that is objectively measured and evaluated as an indicator of normal biological processes, pathogenic processes, or pharmacologic responses to a therapeutic intervention (Atkinson et al., 2001).” In the case of SCAs, biomarkers are needed to detect early neurodegenerative changes preceding ataxia

onset, because the existing clinical outcome measures are not sensitive in the non-ataxic stage.

For SCA3, there is no need for a diagnostic biomarker, since the mutation detection is the definitive diagnostic marker. Other than that, CAG repeat counts and other modifiers of age of onset, especially the ATXN3 levels in CSF, polyQ positron emission tomography (PET), serum Neurofilament light (NfL) and MRI are considered as candidate biomarkers. Different MRI sequences are used to show different aspects of pathogenesis: T1 weighted MRI for macrostructural changes, magnetic resonance spectroscopy (MRS) for neurochemical alterations by measuring the concentration of *N*-acetylaspartate (NAA), a marker of neuronal integrity and finally, diffusion MRI or diffusion tensor imaging (DTI) allowing the detection of microstructural changes in the white matter.

MRI based biomarkers have already proved their efficacy in various studies. In a multicenter longitudinal 2 year follow up study with SCA1, SCA3 and SCA6 patients (EUROSCA), MRI measures were found to be even more sensitive to change than the most sensitive clinical outcome measure. MR volumetry revealed volume loss of cerebellum, brainstem and basal ganglia in all genotypes. Longitudinal voxel based morphometry (VBM) revealed grey matter loss in cerebellum, brainstem, basal ganglia and thalamus (Reetz et al., 2013). In a cross-sectional study with 38 SCA3 patients, VBM showed grey and white matter loss in cerebellum and brainstem, whereas DTI metrics were altered in cerebellum, brainstem, thalamus, frontal and temporal lobes (Guimarães et al., 2013). In a SCA cohort with 100 subjects with a SARA score < 10, neurochemical abnormalities were detectable by MRS already in the non-ataxic stage up to 10 years before the calculated age of onset (Joers et al., 2018). Based on these previous studies, MRI seems to be a very good biomarker candidate that can be utilized for patient selection, treatment monitoring and as a safety marker (Ashizawa et al., 2018).

1.6.5 Objective

SCA3 patients show atrophy of the cervical spinal cord. The extent of cervical spinal cord atrophy correlates with the ataxia severity (SARA) as well as disease duration (Fahl et al., 2015; Lukas et al., 2008; Rezende et al., 2018). Therefore, cervical spinal cord alteration is a promising MR biomarker candidate in SCA3. Our aim was to investigate the upper cervical spinal cord morphometry in a large multicenter, cross sectional cohort of ataxic and non-ataxic SCA3 mutation carriers and healthy controls. Our hypotheses were:

- Cervical spinal cord atrophy is already present in non-ataxic mutation carriers.
- Cervical spinal cord atrophy in the ataxic disease stage is correlated to disease severity (SARA).
- Cervical spinal cord atrophy is progressive throughout the whole course of the disease.

The analysis of spinal cord morphometry has become more prominent within the last few years. By now, software packages are available that allow analysis of large cohort collections. In the conducted previous pilot analysis, the automated segmentations of the spine using these software packages was too inaccurate. Delineation of the spinal cord and the automated positioning of cervical levels failed in a relevant number of cases. So, finally, we decided to prove the above mentioned hypotheses by applying existing software packages and manual segmentations in parallel.

2. Materials and methods

2.1 General Characteristics of the Cohort

The European Spinocerebellar Ataxia Type 3/Machado Joseph Disease Initiative (ESMI) has been initiated with the idea to bring existing cohorts of SCA3 mutation carriers together, to develop new disease markers to build up a trial ready cohort for future interventional trials. Within the prospective part, standardized and quality-controlled assessment protocols including clinical scales, biosampling and MRI were applied. Within the retrospective part, existing data were integrated into a common database and pooled for a cross-sectional analysis.

2.2 Participants

All patient and healthy control subject data were provided by ESMI partners and collaborating sites as part of the retrospective analysis within ESMI. The examinations were carried out on the basis of the revised Helsinki Declaration of the World Medical Association (1983) and the corresponding legal basis.

Data included T1 weighted MRI and a basic subset of clinical information as follows: age at scan, gender and for patients in addition a score to measure disease severity (Sum score of the Scale for the Assessment and Rating of Ataxia, (SARA)), age of onset, defined as the first appearance of gait disturbances and the repeat length of the longer allele as genetic information. Disease duration was calculated as the time from age of onset to age at scan in years. All participants gave their written informed consent for the research use of their clinical and MRI data. 214 data sets were included in our cross-sectional cohort. 29 scans had to be excluded due to various reasons such as: incomplete scans lacking the C2/C3 level, neck anteflexion/retroflexion during scan, chronic neck pathologies such as kyphosis or torticollis which would cause a pseudo-atrophy in manual volumetry or motion artifacts.

Finally 153 SCA3 mutation carriers as well as 32 healthy controls were included in the analysis from sites in Brazil, China and Europe (Germany (Bonn, Essen, Frankfurt, Tübingen), the Netherlands (Nijmegen), France (Paris) and Spain (Santander)), for details see **Tab. 1.**

2.3 Clinical Scale

The Scale for the Assessment and Rating of Ataxia (SARA) is a well established scale to assess the severity of ataxic symptoms (Schmitz-Hübsch et al., 2006). It is a semiquantitative scale, taking about 10 minutes to apply for an experienced clinician. SARA is composed of 8 items: evaluation of gait (score 0–8), stance (score 0–6), sitting (score 0–4) and speech (score 0–6), and four tests assessing limb kinetic function (finger chase (score 0–4), fast alternating hand movements (score 0–4), finger–nose–finger test (score 0–4) and heel–shin test (score 0–4)). SARA sum scores range from 0, for a normal examination, to 40.

2.4 Group Definition

We categorized the SCA3 mutation carriers based on the suggestions of Jacobi et al. using a SARA cut-off value of 3 to define the non-ataxic group (defined by a SARA less than 3) versus the ataxic group (SARA equal or higher than 3) of mutation carriers (Jacobi et al., 2015).

2.5 Imaging Acquisition

For this retrospective approach, all participating sites were asked to contribute T1 weighted scans without restrictions to the imaging acquisition or protocol despite the exclusion of contrast-medium enhanced MRI and a slice-thickness of less than 1.5mm for all directions. No other MRI conditions regarding vendor, direction of acquisition or

sequence parameters like echo time, repetition time etc. were predefined to include all available scans and define a mixed data set including scans acquired within research and clinical settings.

2.6 Cervical Spinal Cord Volumetry

Cervical spinal cord alterations have been discussed to reflect early changes in SCA3 mutation carriers. To assess cervical spinal cord morphometry, we chose different methodological approaches: manual delineation of the cross-sectional area, anterior-posterior and left-right diameter at the intervertebral level between 2nd and 3rd cervical vertebrae and a semiautomated approach, in which additionally the volume of the whole cervical spinal cord on the vertebral level 2 and 3 is included.

We used established software packages for imaging analysis. For manual delineation and manual correction steps in the semiautomated analysis we used FreeSurfer (Version 5.3.0) and Spinal Cord Toolbox (SCT, version 3.2.7). Instead of FreeSurfer (Version 5.3.0) as in manual delineation, we used FMRIB Software Library (FSL, version 3.2.0) and ITK-SNAP (version 3.2.0) for manual correction due to their ease of use at editing segmentation and labels.

2.7 Manual Delineation

First, the midsagittal slice of each scan was used to identify the intervertebral disc between cervical vertebrae 2 and 3 (C2/3). The middle of this intervertebral disc in z-direction was used as the C2/C3 level axial slice. **(Fig. 6)** Imaging display properties like contrast and brightness were only changed if necessary. Subsequently, the cross sectional area of the C2/C3 level in the axial view was manually traced as the target region of interest. Finally, we measured the anteroposterior diameter (AP), measured as the midsagittal extent of the spinal cord, and the left-to-right diameter (LR) measured at

the broadest cervical spinal cord extend orthogonal to the sagittal axis (in the following sections for simplification named as “midcoronal”). **(Fig. 7)**

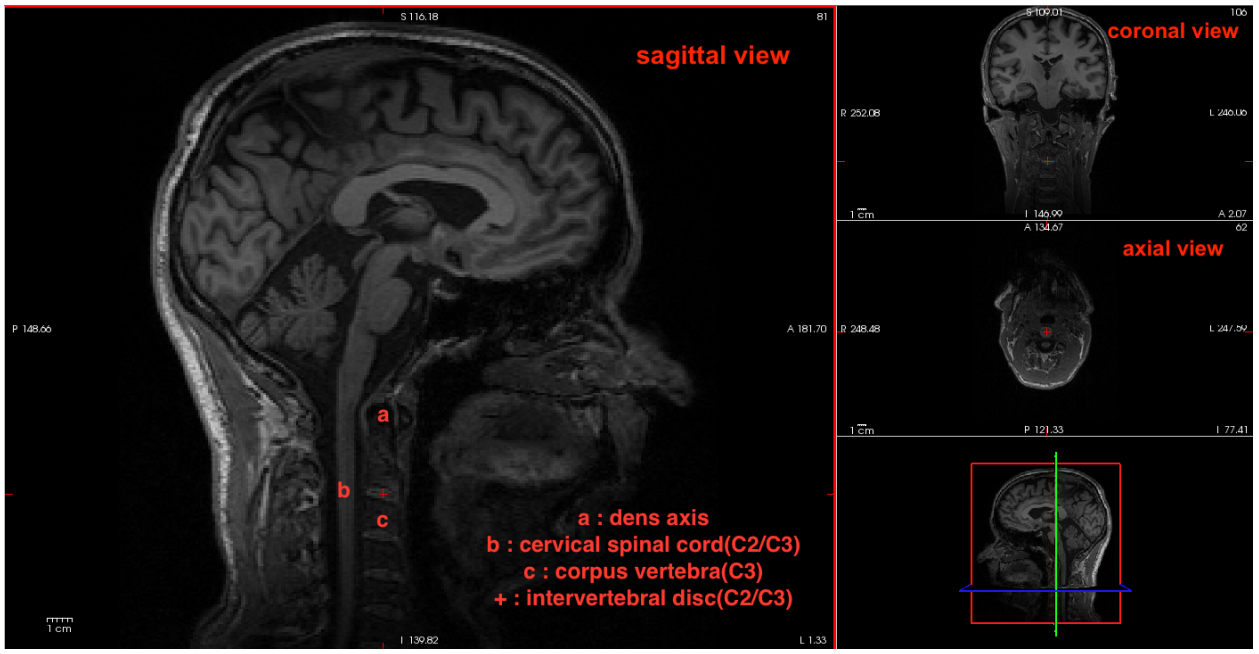

Fig. 6: Identification of C2/C3 level. The first step of the manual delineation was the identification of the C2/C3 level of the cervical spinal cord on the midsagittal slice. Here we show a screenshot of the Freesurfer display as used in the analysis. Dens axis (a), corpus vertebrae C3 (c), cervical spinal cord level C2/C3 (b) and the intervertebral disc at the level between C2 and C3 (+) are marked for anatomical reference.

2.8 Semi-automated Segmentation

The Spinal Cord Toolbox (SCT) software can be used to generate various outputs, e.g. delineation of the centerline of the spinal cord, a segmentation of the whole spinal cord and a vertebrae level related labeling of the spinal cord. As input, raw T1 weighted images can be used. Algorithmic segmentation is challenging, due to similar image intensities of the tissues surrounding the spinal cord, especially of the meninges. Another drawback would be the lower image quality in the neck for MRI images centered to the brain as the main focus, since this portion is far from the view center. Segmentation accuracy can essentially be improved if smoothing is performed in advance and if rough anatomical information is fed into the analysis. Therefore, in our

approach we added the following preprocessing: At first, we manually set the central points of the cervical spine on each intervertebral disc level and second, we used the integrated SCT smoothing option, which applies a Gaussian kernel of 3 voxel in superior-inferior direction. After those preprocessing steps, we generated a centerline and the segmentation of the spinal cord. **(Fig. 8)**

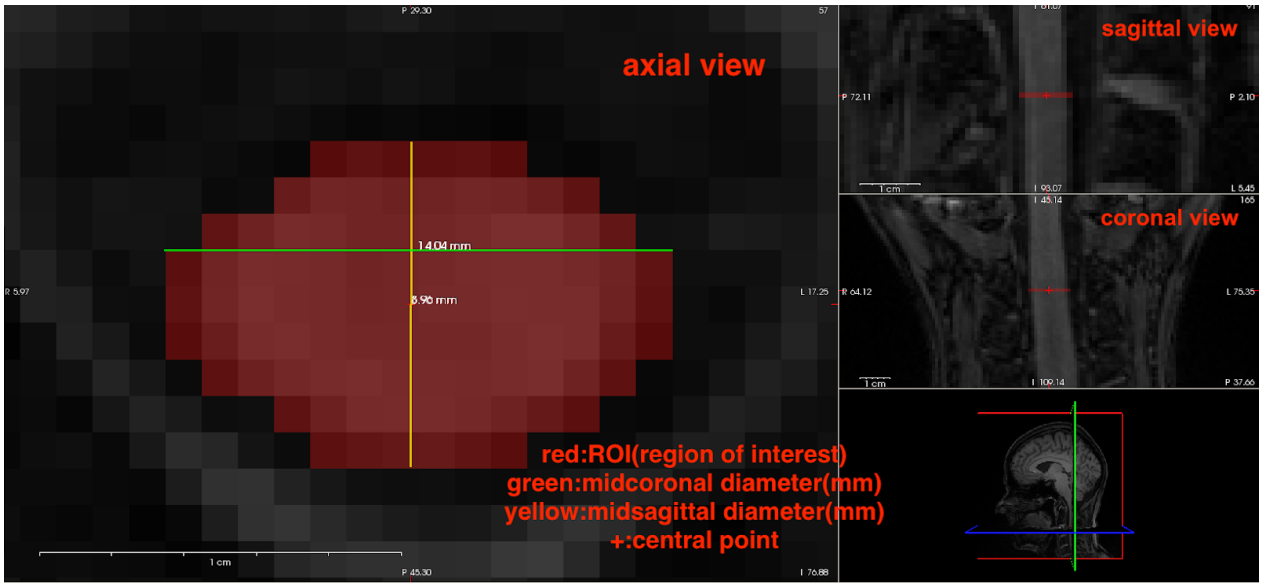

Fig. 7: Delineation of the cross sectional area (CSA) and the left-right (LR) and anteroposterior (AP) diameter at the C2/C3 level. Here we show a screenshot of the freesurfer display as used in the analysis. The axial view in the main window represents the C2/C3 level identified in the previous step. The cross sectional area was delineated as the region of interest (ROI). The midsagittal and midcoronal diameter are given in mm. The "+" is the central reference point, indicating the position for all views (axial, sagittal and coronal view) in the image display and does not refer to any anatomical structure.

The preprocessing of smoothing and manual rough delineation of the centerline improved the accuracy of the segmentation in our cohort essentially. However, even after inclusion of these preprocessing procedures, over- or under segmentation occurred at some levels in more than half of the scans. All scans were inspected and segmentation failures were manually corrected. **(Fig. 9)**

SCT results provide cross sectional area and anteroposterior and left-right-diameter of the spinal cord along the z-axis adjusted for the angle between z-axis and spinal cord centerline at each plane. This is a divergence to the manual approach: In the manual delineation, axial slices were accepted without taking into account the anatomical curvature of the cervical spinal cord, which might result in oblique cut end, not exactly orthogonal to the principal direction of the spinal cord, with an overestimation. SCT results represent the above-mentioned parameters (cross sectional area and diameters) on sections orthogonal to the principal direction of the spinal cord as defined by the centerline.

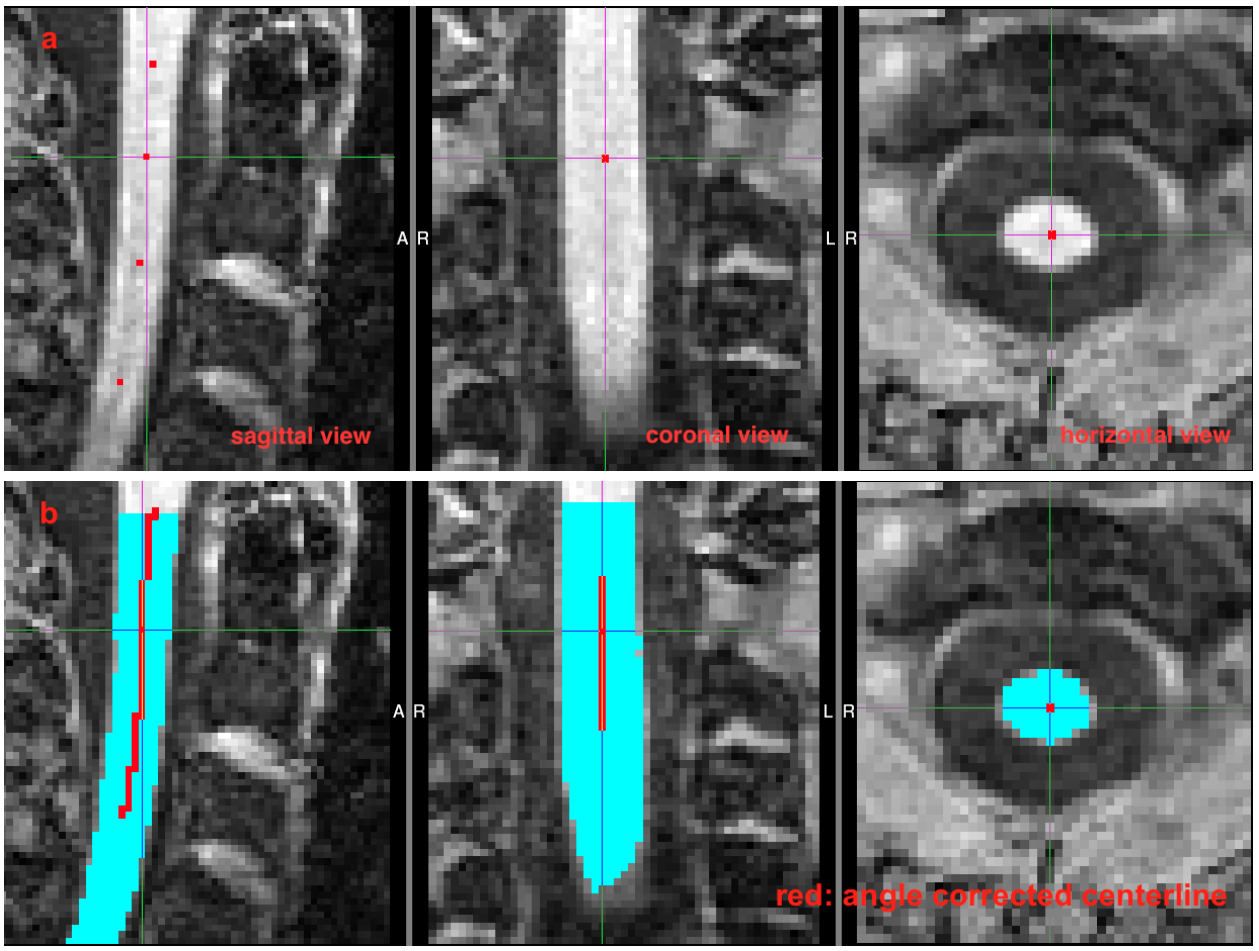

Fig. 8: Semi-automated segmentation of the spinal cord. The preprocessing step of manual identification of the central point of the spinal cord on each intervertebral level in one scan is shown in the upper row (a). The second row shows the segmentation of the spinal cord in light blue and the centerline of the spinal cord in red in the same scan (b). In this subject no manual correction of the SCT segmentation was necessary.

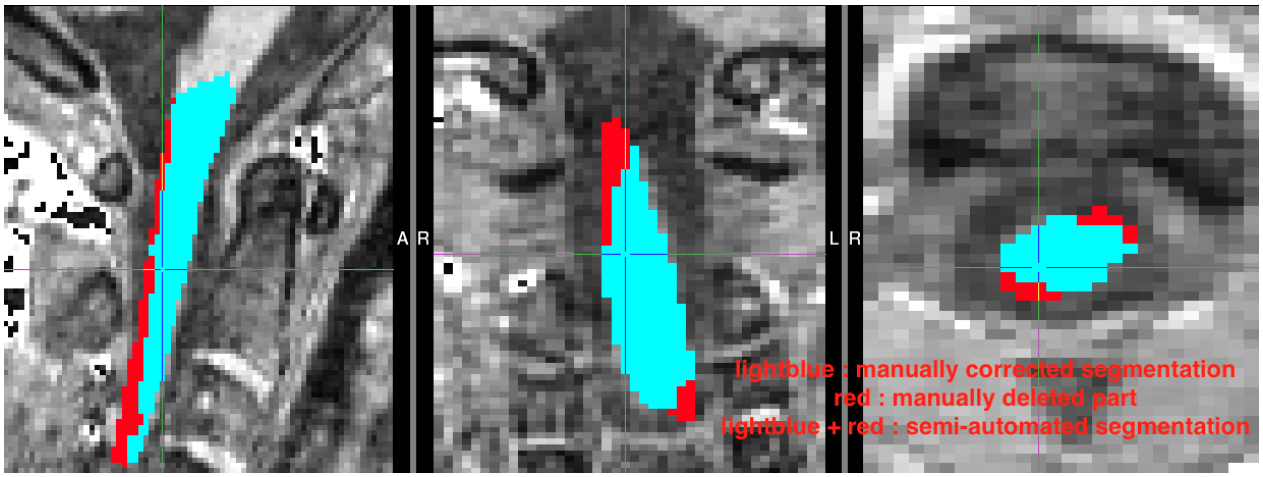

Fig. 9: Manual correction of the semi-automated segment. Example for an over-segmentation. Manually deleted sections of the initial segmentation are coloured in red, the manually corrected segmentation that was used for the final analysis is coloured in light blue.

2.9 Statistical Analysis

For the statistical analysis we used IBM SPSS Statistics 23.0. Group differences in the imaging parameters (CSA, AP, LR) tested by ANCOVA, including the covariates age, sex and site of MRI scan, were considered as significant at a level of significance $p<0.05$. Bonferroni corrected results at a level of significance $p<0.01$ were considered as significant.

To test correlation of the imaging parameters (CSA, AP, LR) with SARA score, age of onset, disease duration, estimated time to disease onset and CAG repeat length of longer allele; Spearmen Test is applied. Results at a level of significance $p<0.05$ were considered as significant.

3. Results

An overview of all demographic and clinical data of the study population can be found in **Tab. 1**. Our study group is a gender-balanced population of 92 males (49.7%) and 93 females (50.3%), consisting predominantly of ataxic populations (65%) gathered from European cohorts (54.6%). Age at onset in this cross-sectional study ranged from 4th to 6th decades. As expected, non-ataxic mutation carriers (mean age 39 years) were significantly younger than ataxic mutation carriers (mean age 46 years) **(Tab. 2)**. The calculated age at disease onset, with a mean of 48.73 years, showed a substantially later disease onset than in the ataxic population, with a mean of 37.38 years.

Tab. 1: Demographic information and clinical scales

		HC (N=32)	NA (N=33)	A (N=120)	Total (N=185)
Sex (N, (%))	**male**	17 (53.1 %)	15 (45.5 %)	60 (50 %)	92 (49.7 %)
	female	15 (46.9 %)	18 (54.5 %)	60 (50 %)	93 (50.3 %)
Site (N, (%))	**Brazil**	0	2 (6.1 %)	33 (27.5 %)	35 (18.9 %)
	China	0	0	49 (40.8 %)	49 (26.5 %)
	Europe	32 (100 %)	31 (93.9 %)	38 (31.7 %)	101(54.6 %)
SARA sum score (mean (SD))		0.17 (0.53)	1.33 (0.98)	12.48 (5.81)	8.37 (7.33)
CAG repeat length of longer allele (mean, (SD))		n.a.	67.27 (2.66)	72.03 (4.09)	71 (4.29)
Age at scan (mean (SD))		42.84 (13.47)	39.03 (8.97)	46.01 (11.40)	44.22 (11.66)
Age of disease onset (mean (SD))		n.a.	n.a.	37.38 (10.34) (n=120)	37.38 (10.34) (n=120)
Calculated age of disease onset (mean, (SD))		n.a.	48.73 (8.18)	n.a.	n.a.
Disease duration in years (mean, (SD))		n.a.	n.a	8.46 (4.54) (n=120)	8.46 (4.54) (n=120)
Estimated time to disease duration in years (mean, (SD))		n.a.	-10 (4.07)	n.a.	n.a.
HC: Healthy controls, NA: non-ataxic mutation carriers, A: ataxic mutation carriers					

Tab. 2: ANOVA test for group differences in the age at scan date

Contrast	p-value *
HC vs. NA	0.538
HC vs. A	0.494
NA vs. A	**0.006****
* Bonferroni-corrected for multiple comparisons * *The mean difference is significant at the level p < 0.01. HC: Healthy controls, NA: non-ataxic mutation carriers, A: ataxic mutation carriers	

The results for both manual and semi-automatic delineation were strongly correlated, with R2 coefficients ranging from 0.453 to 0.641, with the semiautomatic approach yielding distinctly lower values. (12.5% lower for AP, 7.9% lower for LR, and 26.8% lower for CSA). **(Fig. 10-12) (Tab. 3-5)**

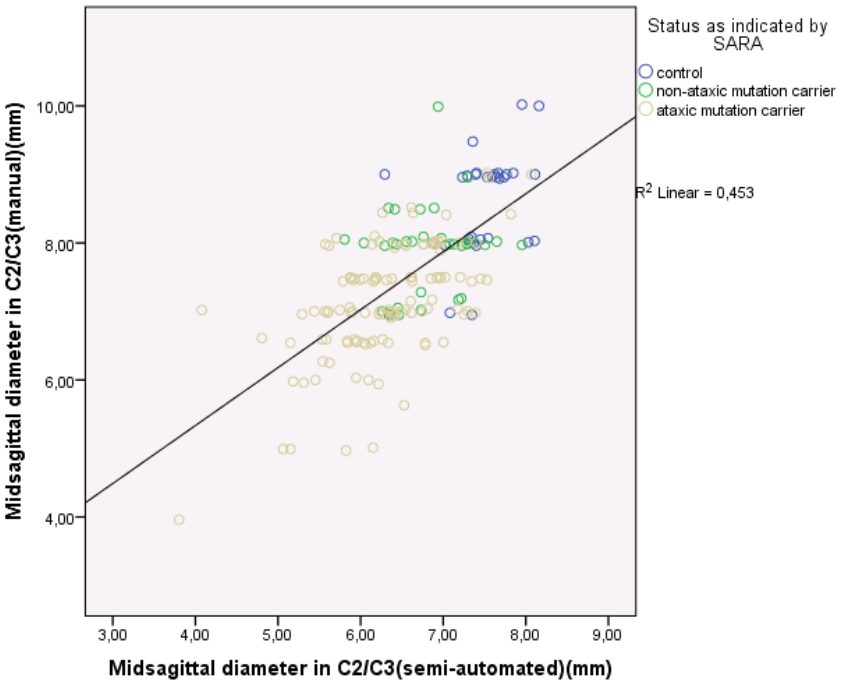

Fig. 10: Scatter plot showing the comparison between semi-automated (x-axis) and manual (y-axis) approaches for anteroposterior (AP) diameter at C2/C3 in mm. Value pairs of healthy controls, non-ataxic and ataxic mutation carriers are coloured in blue, green and brown respectively.

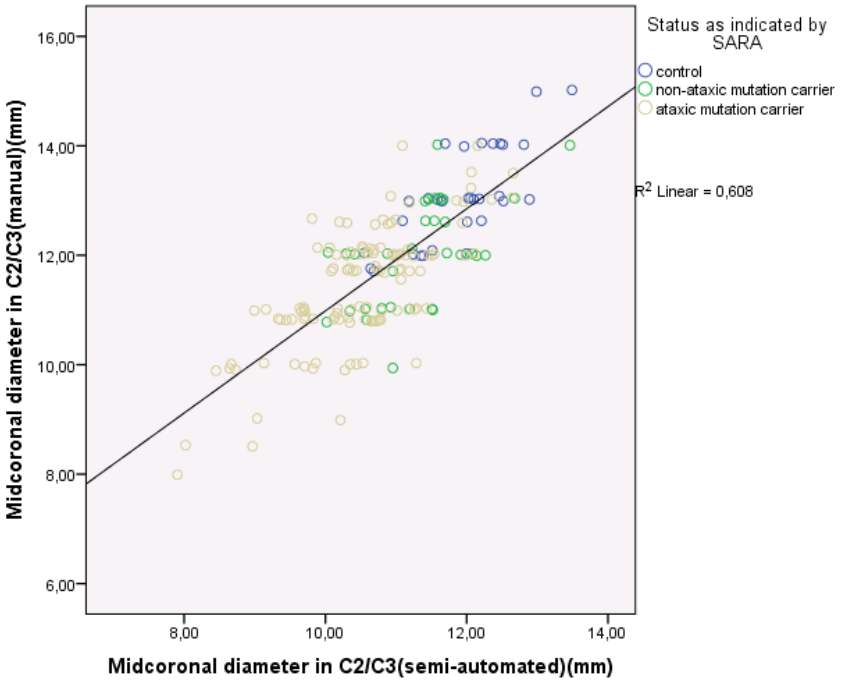

Fig. 11: Scatter plot showing the comparison between semi-automated (x-axis) and manual (y-axis) approach for left to right (LR) diameter at C2/C3 in mm. Value pairs of healthy controls, non-ataxic and ataxic mutation carriers are coloured in blue, green and brown respectively.

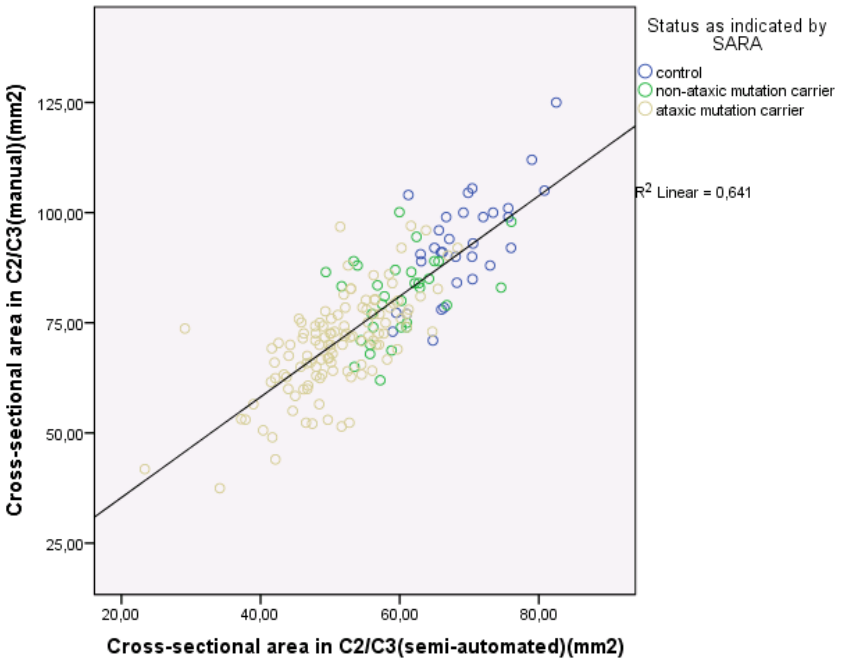

Fig. 12: Scatter plot showing the comparison between semi-automated (x-axis) and manual (y-axis) approach for cross-sectional area (CSA) in C2/C3 in mm². Value pairs of healthy controls, non-ataxic and ataxic mutation carriers are coloured in blue, green and brown respectively.

The mean values of anteroposterior (AP) and left-right diameter (LR) as well as the cross sectional area (CSA) at the C2/C3 level were in descending order from healthy controls to non-ataxic mutation carriers and lastly to ataxic mutation carriers, exhibiting progressive atrophy of spinal cord. **(Fig. 13-15, Tab. 3-5)**

Tab. 3: AP at C2/C3 in mm

Status as indicated by SARA		Mean	SD
HC	**Manual**	8.54	0.78
	Semi-automated	7.46	0.44
NA	**Manual**	7.96	0.65
	Semi-automated	6.82	0.50
A	**Manual**	7.18	0.85
	Semi-automated	6.32	0.71
HC: Healthy controls, NA: non-ataxic mutation carriers, A: ataxic mutation carriers			

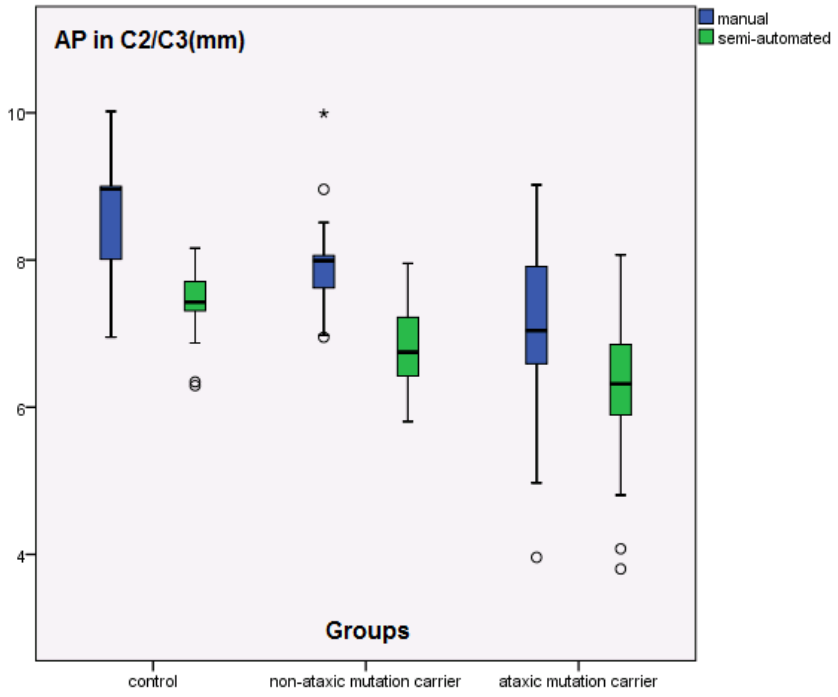

Fig. 13: Box plot showing the anteroposterior (AP) diameter at C2/C3 in mm for the groups of healthy controls, non-ataxic and ataxic mutation carriers. The results of the manual segmentation are shown in blue and of the semi-automated approach in green for each group. Circles indicate outliers with values between 1.5 and 3 times the interquartile range, whereas asterisks indicate extreme outliers with values of more than 3 times the interquartile range.

Tab. 4: LR at C2/C3 in mm

Status as indicated by SARA		Mean	SD
HC	Manual	13.06	0.89
	Semi-automated	11.90	0.70
NA	Manual	12.03	0.96
	Semi-automated	11.33	0.76
A	Manual	11.43	1.11
	Semi-automated	10.50	0.91
HC: Healthy controls, NA: non-ataxic mutation carriers, A: ataxic mutation carriers			

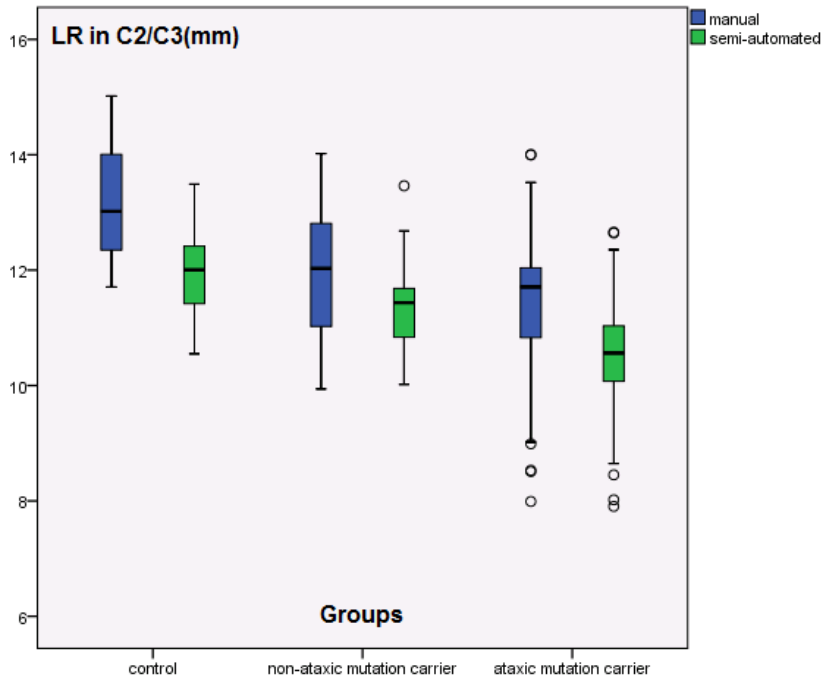

Fig. 14: Box plot showing the left to right (LR) diameter at C2/C3 in mm for the groups of healthy controls, non-ataxic and ataxic mutation carriers. The results of the manual segmentation are shown in blue and of the semi-automated approach in green for each group. Circles indicate outliers with values between 1.5 and 3 times the interquartile range, whereas asterisks indicate an extreme outlier with values more than 3 times the interquartile range.

Tab. 5: CSA at C2/C3 in mm^2

Status as indicated by SARA		Mean	SD
HC	**Manual**	92.94	11.73
	Semi-automated	68.93	5.92
NA	**Manual**	80.92	9.01
	Semi-automated	59.81	5.83
A	**Manual**	70.17	10.98
	Semi-automated	50.96	7.32
HC: Healthy controls, NA: non-ataxic mutation carriers, A: ataxic mutation carriers			

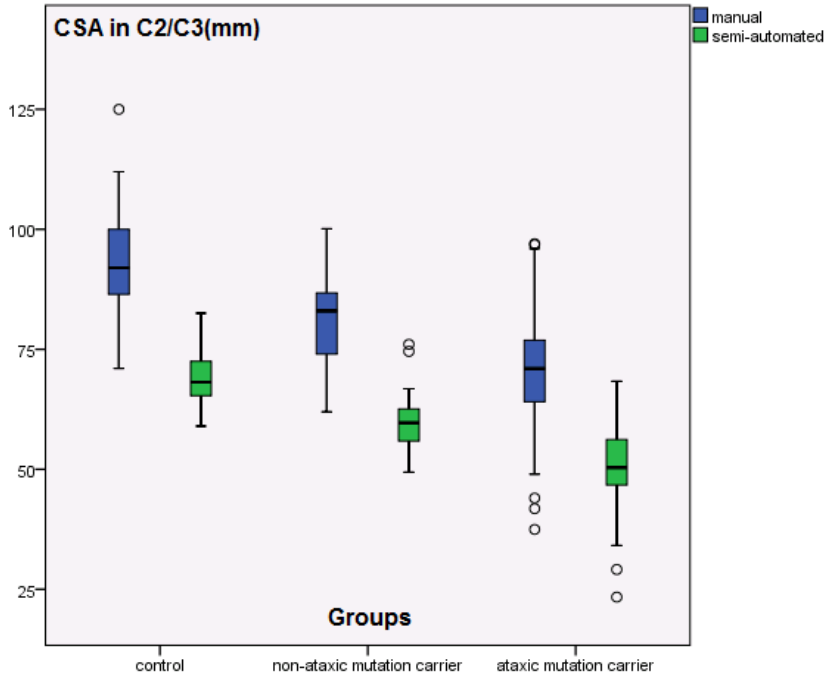

Fig. 15: Box plot showing the cross-sectional area (CSA) at C2/C3 in mm^2 for the groups of healthy controls, non-ataxic and ataxic mutation carriers. The results of the manual segmentation are shown in blue and of the semi-automated approach in green for each group. Circles indicate outliers with values between 1.5 and 3 times the interquartile range, whereas asterisks indicate an extreme outlier with values more than 3 times the interquartile range.

This progressive spinal cord atrophy was further reinforced by the significant ($p<0.05$) group differences in the ANCOVA model for all three parameters (AP, LR, CSA), except for the LR difference between non-ataxic and ataxic mutation carriers, which still showed a trend as the group difference was significant without Bonferroni correction. **(Tab. 6-8)**

Tab. 6: ANCOVA with post-hoc pairwise comparisons for AP at C2/C3

Contrasts	Manual	Semi automated
	Sig.*	Sig.*
HC vs. NA	0.023	0.001
HC vs. A	0.001	0.001
NA vs. A	0.001	0.003
Included covariates: age, sex, site HC: Healthy controls, NA:non-ataxic mutation carriers, A: ataxic mutation carriers * after Bonferroni-correction in post-hoc analysis		

Tab. 7: ANCOVA with post-hoc pairwise comparisons for LR at C2/C3

Contrasts	Manual	Semi automated
	Sig.*	Sig.*
HC vs. NA	0.001	0.026
HC vs. A	0.001	0.001
NA vs. A	0.057#	0.001
Included covariates: age, sex, site HC: Healthy controls, NA:non-ataxic mutation carriers, A: ataxic mutation carriers * after Bonferroni-correction in post-hoc analysis # without Bonferroni correction in post-hoc analysis p=0,019		

Tab. 8: ANCOVA with post-hoc pairwise comparisons for CSA at C2/C3

Contrasts	Manual	Semi automated
	Sig.*	Sig.*
HC vs. NA	0.001	0.001
HC vs. A	0.001	0.001
NA vs. A	0.001	0.001
Included covariates: age, sex, site HC: Healthy controls, NA:non-ataxic mutation carriers, A: ataxic mutation carriers * after Bonferroni-correction in post-hoc analysis		

Spearman test results revealed:

- significant inverse correlation between SARA score and AP, LR, and CSA **(Tab. 9) (Fig. 16-18)**; disease duration and AP, CSA **(Tab. 11)**; repeat length of the longer allele and CSA, semi-automated LR **(Tab. 13)**

- significant positive correlation between estimated time to disease onset and semi-automated AP and CSA **(Tab. 12)**

- no significant correlation as to age of onset **(Tab. 10)**

Tab. 9: Correlation with SARA

	AP (manual)	AP (semi-automated)	LR (manual)	LR (semi-automated)	CSA (manual)	CSA (semi-automated)
Correlation coefficient	-0.404**	-0.353**	-0.159*	-0.307**	-0.363**	-0.483**
Sig.	**0.001**	**0.001**	0.049	**0.001**	**0.001**	**0.001**
* The correlation is significant at a level of p<0.05. ** The correlation is significant at a level of p<0.01.						

Tab. 10: Correlation with Age of Onset

	AP (manual)	AP (semi-automated)	LR (manual)	LR (semi-automated)	CSA (manual)	CSA (semi-automated)
Correlation coefficient	0.002	-0.038	0.140	0.131	0.043	0.006
Sig.	0.985	0.674	0.119	0.150	0.633	0.950

Tab. 11: Correlation with Disease Duration

	AP (manual)	AP (semi-automated)	LR (manual)	LR (semi-automated)	CSA (manual)	CSA (semi-automated)
Correlation coefficient	-0.191	-0.191	-0.068	-0.119	-0.209	-0.257**
Sig.	**0.034**	**0.034**	0.449	0.191	**0.020**	**0.004**
** The correlation is significant at a level of p<0.01.						

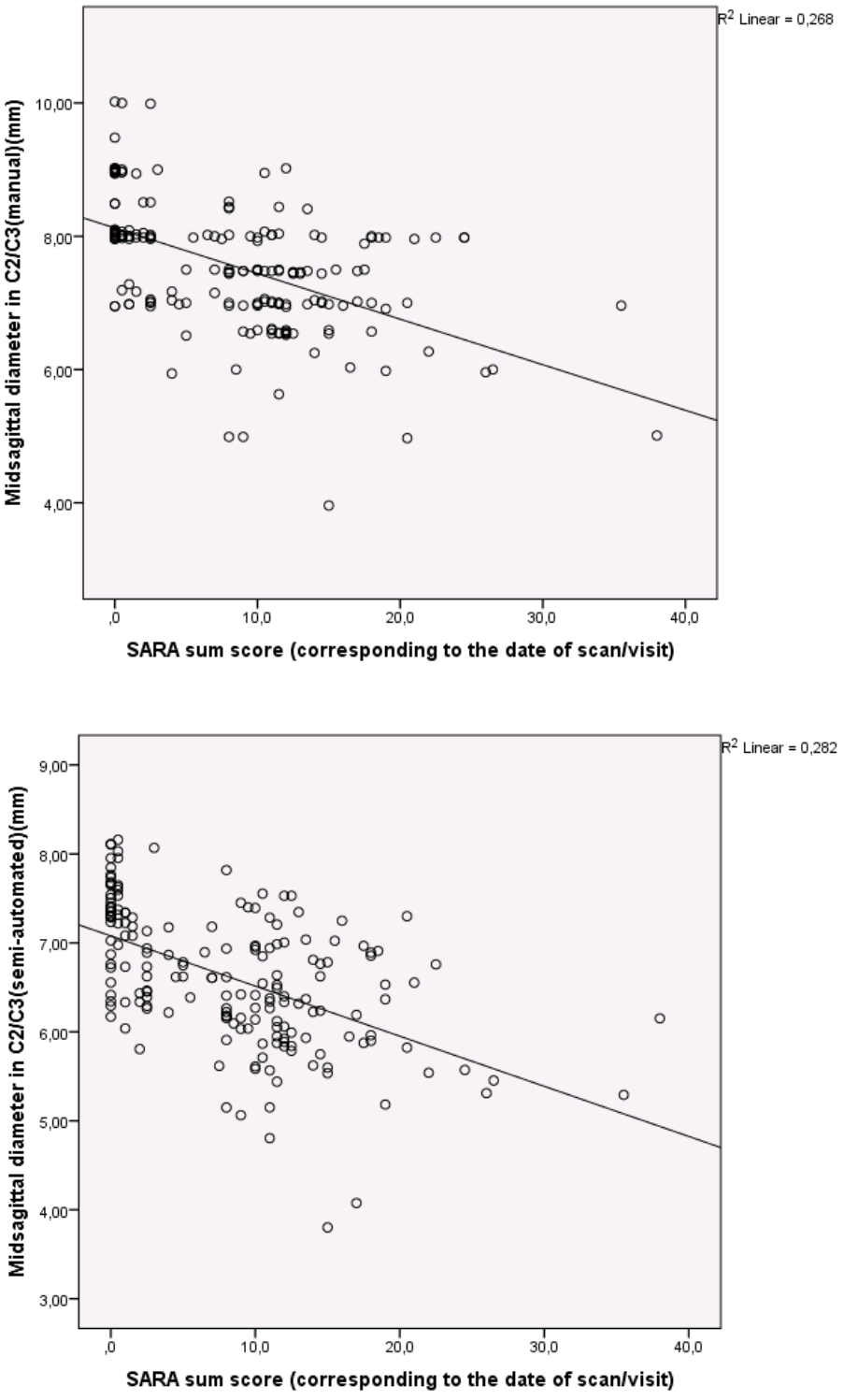

Fig. 16: Scatter Plots - SARA vs. Midsagittal diameter (AP). The top diagram shows the values of the manual delineation, the bottom diagram of the semi-automated volumetry.

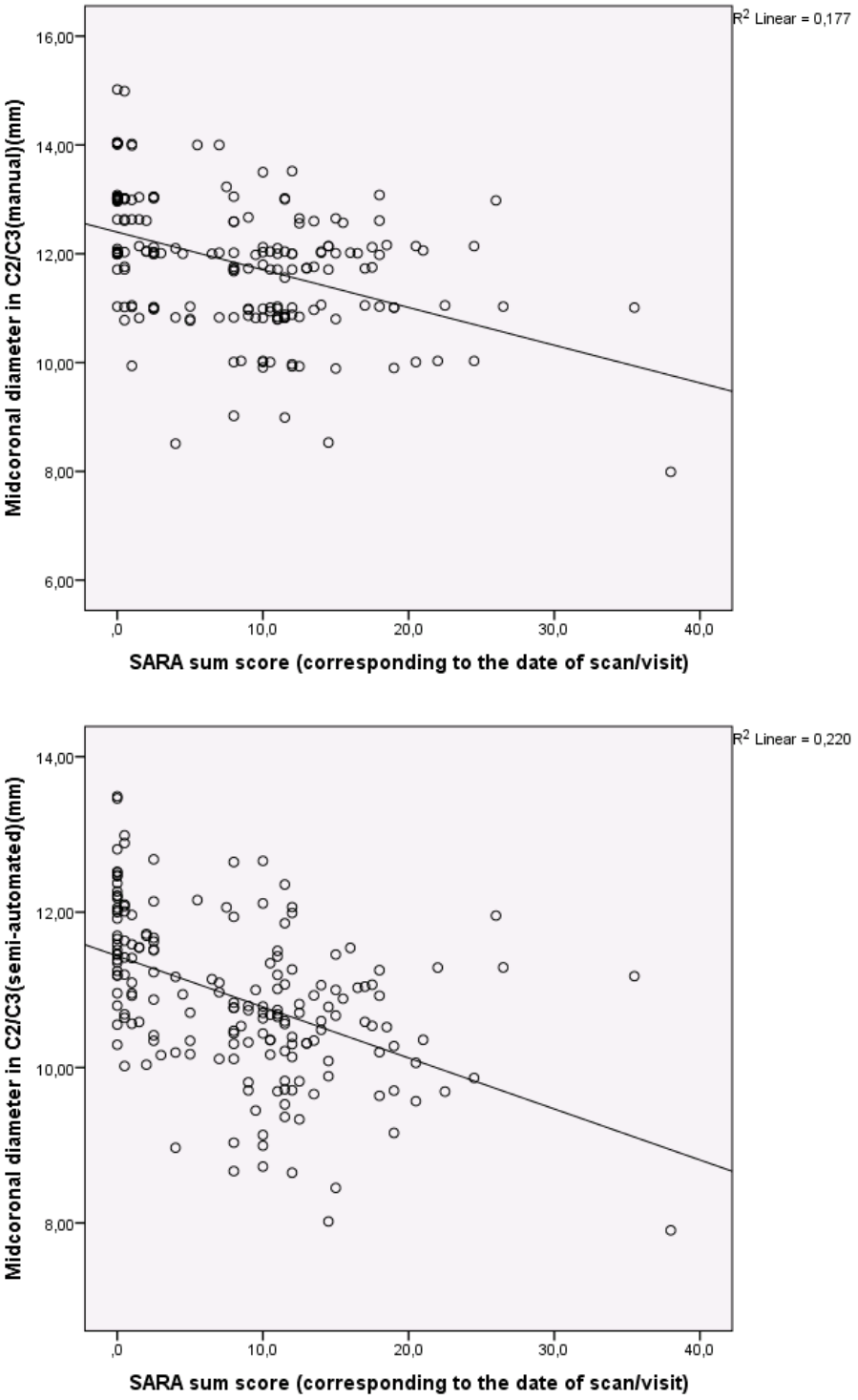

Fig. 17: Scatter Plots - SARA vs. Midcoronal diameter (LR). The top diagram shows the values of the manual delineation, the bottom diagram of the semi-automated volumetry.

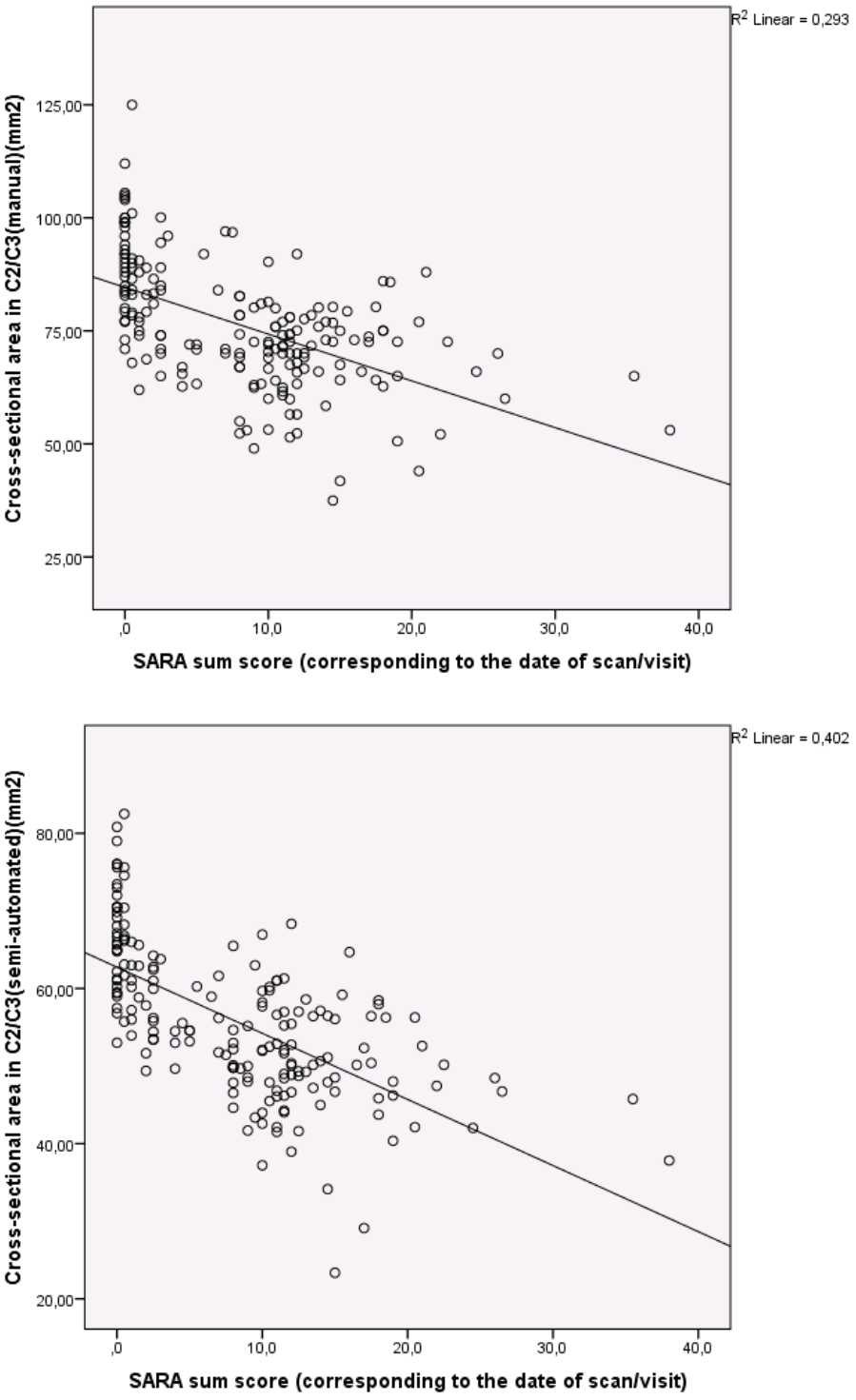

Fig. 18: Scatter Plots - SARA vs. Cross-sectional area (CSA). The top diagram shows values of the manual delineation, the bottom diagram of the semi-automated volumetry.

Tab. 12: Correlation with Estimated Time to Disease Onset

	AP (manual)	AP (semi-automated)	LR (manual)	LR (semi-automated)	CSA (manual)	CSA (semi-automated)
Correlation coefficient	0.265	0.493**	0.157	0.002	0.336	0.473**
Sig.	0.157	**0.006**	0.408	0.992	0.070	**0.008**
** The correlation is significant at a level of p<0.01.						

Tab. 13: Spearman Test – Correlation with CAG repeat length of longer allele

	AP (manual)	AP (semi-automated)	LR (manual)	LR (semi-automated)	CSA (manual)	CSA (semi-automated)
Correlation coefficient	-0.137	-0.119	-0.156	-0.222**	-0.176	-0.225**
Sig.	0.092	0.145	0.055	**0.006**	**0.030**	**0.006**
** The correlation is significant at a level of 0.01.						

4. Discussion

Our data clearly show atrophy of the upper cervical spinal cord in SCA3 mutation carriers, already present in the pre-ataxic disease stage before the clinical onset of the disease. Atrophy of the upper cervical spinal cord was most prominent in later, ataxic disease stages and correlated with disease severity, assessed by SARA, and disease duration. Anteroposterior (AP) as well as left-right diameter (LR) and cross-sectional area (CSA) at the level of C2/C3 were in descending order from healthy controls to non-ataxic mutation carriers and finally to ataxic mutation carriers.

A strength of our study is the large cohort of patients suffering from a rare disease, including a high number of presymptomatic, non-ataxic mutation carriers. However, the relatively low number of control subjects did not allow age and gender matching, and the groups were imbalanced over the sites.

Previous studies in smaller groups of SCA3 mutation carriers have shown cerebellar and cerebral atrophy and atrophy in the upper cervical spinal cord (Bürk et al., 1996; Fahl et al., 2015; Lukas et al., 2008; Rezende et al. 2018; Wüllner et al. 1993). Our results are in line with these previous results, demonstrating atrophy in pre-ataxic and ataxic SCA3 mutation carriers. In our cohort; CSA, AP and LR of the cervical spinal cord at the vertebral level C2/C3 showed highly significant group differences between non-ataxic and ataxic mutation carriers in comparison to healthy controls and also between non-ataxic and ataxic mutation carriers. Interestingly, AP and CSA displayed higher correlation coefficient values with SARA score, disease duration and estimated time to disease onset than LR. These results might be a hint for a more anteroposterior flattening of the spinal cord, which has previously been suggested by Fahl et al.(2015) and Martins et al.(2017), not only in SCA3 but also in SCA1 subjects.

Previous studies showed a clear dependence of the age of onset on the repeat length (Durr et al., 1996). Our results showed a significant correlation of the investigated morphometric parameters with repeat length, however not with the age of onset, which was somehow surprising. A potential explanation could be that the repeat length is a parameter that reflects the underlying disease pathology more directly, whereas age of

onset and morphometry are dependent variables not necessarily directly linked. Nevertheless, similar results have been shown in SCA1 in the study of Martins et al. (2017), indicating a correlation between CSA at C2/C3 level and repeat length as well as disease duration.

Huntington's disease is the most common and well-studied of the polyglutamine diseases; characterized by CAG trinucleotide repeat expansion in the huntingtin (*HTT*) gene, which encodes huntingtin protein (HTT). Gene silencing therapies such as antisense oligonucleotides(ASO) bear a great therapeutic potential for Huntington´ disease(HD). In a recent interventional phase I/IIa trial, intrathecal injection of an antisense oligonucleotide drug showed a dose-dependent reduction of mutated HTT protein levels in cerebrospinal fluid (Tabrizi et al., 2019). The development of analogue therapeutic approaches in SCA3 is on the horizon. For a drug that addresses the underlying genetic pathology, the early symptomatic and presymptomatic disease phases are in the focus of an optimal treatment window.

To assess disease severity and progression in the symptomatic disease stages, the SARA score is a well established scale (Schmitz-Hübsch et al., 2006) with an annual increase of about 1 to 2 points in the symptomatic phase of SCA3 (Jacobi et al., 2015). It has been shown in previous studies in SCA patients, that MRI parameters were even more sensitive to change than clinical scales also in the ataxic stages (Reetz et al., 2013). Our results show a negative correlation of all parameters with SARA sum score, indicating that clinical progression and atrophy of the upper cervical spinal cord go in parallel in the ataxic disease phase.

However, clinical scales like SARA lack sensitivity in the non-ataxic disease stage which emphasizes the importance of imaging biomarkers for this disease stage. In Huntington’s Disease, which – as already mentioned – shares a comparable genetic background with SCA3, structural MRI changes, like e.g. the striatal atrophy also appeared early in the disease course and its decrease was fairly constant and thereby fairly predictable throughout the whole course of the disease (Ross et al., 2014). For future interventional trials, biomarkers especially sensitive in the non-ataxic and early ataxic disease stages are of urgent need. Our data suggest that for SCA3, the cervical

spinal cord morphometry is one core candidate for the pre-ataxic disease phase and might be of additional value to assess disease progression.

From the methodological point of view, we would not recommend a fully automated processing of brain MRI for spinal cord analysis using the SCT software package. We found a high percentage of relevant over- and under segmentation in about one half of the scans that had to be manually corrected. Nevertheless, results for the semi-automated and the manual delineation were highly correlated **(Fig.10-12)**. Manual delineation is a very time consuming process. Therefore, we had to restrict the manual analysis to the investigation of only one cross-section of the cervical spinal cord in the large data set of scans. By using the semi-automated approach, the analysis of not only one cross-section, but the spinal cord morphometry along the whole imaged spine – even when manual inspection and correction are included – was much faster and allowed a more detailed and deepened investigation of additional parameters. However, mean values of the semi-automated method were systematically lower than the mean values of the manual delineation. **(Fig. 13-15, Tab. 3-5)** This difference can be explained geometrically: In the manual delineation, we strictly stuck to the scanner related z-axis, not accounting for any anatomical curvature, whereas cross sections in semi-automated approach were angle corrected. Therefore, CSA of the semi-automated approach should delineate almost the exact cross section, whereas our manual delineation might refer to an oblique (and thereby enlarged) cross section. In other words, results of the manual delineation are based on potentially oblique cuts of the spine, whereas the sections in the semi-automated approach are orthogonal to the spine centerline and thereby almost represent the exact transverse section which per definition is the minimum of all possible cuts. Despite the abovementioned systematic difference, given the high correlation between manual and semi-automated results, we are convinced that a semi-automated approach, when including manual inspection and – if necessary – correction of the automated segmentations is valuable and provides credible results.

Since the main focus of this thesis was the investigation of alterations of the upper cervical spinal cord in SCA3 mutation carriers, we did not extend the methodological comparisons. This needs to be done for further investigations when no manual correction can be performed.

To sum up, our results emphasize that the morphometry of the upper cervical spinal cord is one of the most promising biomarker candidates, reflecting disease pathology and progression throughout the whole course of the disease, especially including non-ataxic stages.

However, because of the cross-sectional nature of our study, we would like to point out that our results will have to be validated by prospective study designs that should ideally include additional cervical spinal cord levels and spine focused imaging. This will be necessary to achieve more insight and a deeper understanding on the suitability of cervical spinal cord atrophy as a valid and sensitive biomarker to be used in future clinical trials in SCA3.

5. Summary

5.1 Objective

Spinocerebellar ataxia Type 3/Machado-Joseph disease (SCA3/MJD) is worldwide the most frequent autosomal dominantly inherited ataxia. Although the gene mutation causing SCA3 is known, there is up to now no treatment available. However, new therapeutic approaches including gene modifying drugs are on the horizon. Therefore, there is an urgent need to identify and validate sensitive biological markers that reflect the individual disease profile. Of particular interest are markers that are already sensitive in the pre-ataxia stage. As SCA3 is associated with widespread cerebellar, cerebral and spinal cord structural alterations, MRI-based spinal cord morphometric measures are promising candidates for such markers. Our aim was to investigate the morphometry of the upper cervical spinal cord in a large cross-sectional cohort of non-ataxic and ataxic SCA3 mutation carriers.

5.2 Methods

We used T1 weighted MRI scans of 33 non-ataxic and 120 ataxic SCA3 mutation carriers and 32 healthy controls to assess the cross sectional area(CSA), anteroposterior(AP) and left-right(LR) diameter of the upper cervical spinal cord at the intervertebral level C2/C3. We applied manual delineation and a semi-automated approach.

5.3 Results

CSA, AP and LR of the cervical spinal cord at the intervertebral level C2/C3 were significantly reduced already in non-ataxic SCA3 mutation carriers in comparison to healthy controls. Atrophy was highest in symptomatic mutation carriers and correlated with disease severity, assessed by SARA, and partially with disease duration and CAG repeat length of the longer allele.

5.4 Conclusion

Our results show that atrophy of the upper cervical spinal cord starts already in the pre-ataxic disease stage, is progressive throughout the whole course of the disease and correlates to disease severity. Therefore, morphometry of the upper cervical spinal cord is a promising MRI biomarker candidate for future interventional trials in SCA3.

6. List of figures

Figure 1: Epidemiological distribution of SCAs 12
Figure 2: Coding and non-coding repeat expansion SCAs 13
Figure 3: Normal and disease repeat lengths for the CAG/polyglutamine diseases 14
Figure 4: Molecular structure and function of ATXN 3 15
Figure 5: RNA toxicity and RAN translation 18
Figure 6: Identification of C2/C3 level 27
Figure 7: Delineation of the cross sectional area(CSA) and the left-right(LR) and anteroposterior(AP) diameter at the C2/C3 level 28
Figure 8: Semi-automated segmentation of the spinal cord 29
Figure 9: Manual correction of semi-automated segment 30
Figure 10: Scatter plot showing the comparison between semi-automated(x axis) and manual(y axis) approaches for anteroposterior (AP) diameter at C2/C3 in mm 32
Figure 11: Scatter plot showing the comparison between semi-automated(x axis) and manual(y axis) approaches for left to right (LR) diameter at C2/C3 in mm 33
Figure 12: Scatter plot showing the comparison between semi-automated(x axis) and manual(y axis) approaches for cross-sectional area (CSA) in C2/C3 in mm² 33
Figure 13: Box plot showing the anteroposterior (AP) diameter at C2/C3 in mm for the control group, non-ataxic and ataxic mutation carriers 34
Figure 14: Box plot showing the left to right (LR) diameter at C2/C3 in mm for the control group, non-ataxic and ataxic mutation carriers 35
Figure 15: Box plot showing the cross-sectional area (CSA) at C2/C3 in mm² for the control group, non-ataxic and ataxic mutation carriers 36
Figure 16: Scatter Plots - SARA vs. Midsagittal diameter (AP) 40
Figure 17: Scatter Plots - SARA vs. Midcoronal diameter (LR) 41
Figure 18: Scatter Plots - SARA vs. Cross-sectional area (CSA) 42

7. List of tables

Table 1: Demographic information and clinical scales 31

Table 2: ANOVA test for group differences in the age at scan date 32

Table 3: AP at C2/C3 in mm 34

Table 4: LR at C2/C3 in mm 35

Table 5: CSA at C2/C3 in mm^2 36

Table 6: ANCOVA with post-hoc pairwise comparisons for AP at C2/C3 37

Table 7: ANCOVA with post-hoc pairwise comparisons for LR at C2/C3 37

Table 8: ANCOVA with post-hoc pairwise comparisons for CSA at C2/C3 38

Table 9: Correlation with SARA 38

Table 10: Correlation with Age of Onset 39

Table 11: Correlation with Disease Duration 39

Table 12: Correlation with Estimated Time to Disease Onset 43

Table 13: Spearman Test – Correlation with CAG repeat length of longer allele 43

8. References

Alves, S., Nascimento-Ferreira, I., Auregan, G., Hassig, R., Dufour, N., Brouillet, E., Lima, M.C.P. de, Hantraye, P., Almeida, L.P. de, and Déglon, N. (2008). Allele-Specific RNA Silencing of Mutant Ataxin-3 Mediates Neuroprotection in a Rat Model of Machado-Joseph Disease. PLOS ONE *3*, e3341

Ashizawa, T., Öz, G., and Paulson, H.L. (2018). Spinocerebellar ataxias: prospects and challenges for therapy development. Nat. Rev. Neurol. *14*, 590–605

Ashraf, N.S., Duarte-Silva, S., Shaw, E.D., Maciel, P., Paulson, H.L., Teixeira-Castro, A., and Costa, M. do C. (2018). Citalopram Reduces Aggregation of ATXN3 in a YAC Transgenic Mouse Model of Machado-Joseph Disease. Mol. Neurobiol

Atkinson, A., Colburn, W., Degruttola, V., Demets, D., Downing, G., Hoth, D., Oates, J., Peck, C., Schooley, R., Spilker, B., Woodcock, J., Zeger, S., (2001). NIH Biomarkers Definitions Working GroupBiomarkers and surrogate endpoints: preferred definitions and conceptual framework. Clin Pharmacol Ther 69: 89-95. Clinical Pharmacology & Therapeutics 69, 89–95

Bettencourt, C., and Lima, M. (2011). Machado-Joseph Disease: from first descriptions to new perspectives. Orphanet J. Rare Dis. *6*, 35

Bürk, K., Abele, M., Fetter, M., Dichgans, J., Skalej, M., Laccone, F., Didierjean, O., Brice, A., Klockgether, T., (1996). Autosomal dominant cerebellar ataxia type I Clinical features and MRI in families with SCA1, SCA2 and SCA3. Brain 119, 1497–1505

do Carmo Costa, M., Luna-Cancalon, K., Fischer, S., Ashraf, N.S., Ouyang, M., Dharia, R.M., Martin-Fishman, L., Yang, Y., Shakkottai, V.G., Davidson, B.L., et al. (2013). Toward RNAi Therapy for the Polyglutamine Disease Machado–Joseph Disease. Mol. Ther. *21*, 1898–1908

Chang, Y.-J., Chou, C.-C., Huang, W.-T., Lu, C.-S., Wong, A.M., and Hsu, M.-J. (2015). Cycling Regimen Induces Spinal Circuitry Plasticity and Improves Leg Muscle Coordination in Individuals With Spinocerebellar Ataxia. Arch. Phys. Med. Rehabil. *96*, 1006–1013

Chen, X., Tang, T.-S., Tu, H., Nelson, O., Pook, M., Hammer, R., Nukina, N., and Bezprozvanny, I. (2008). Deranged calcium signaling and neurodegeneration in spinocerebellar ataxia type 3. J. Neurosci. Off. J. Soc. Neurosci. *28*, 12713–12724

Costa, M. do C., Ashraf, N.S., Fischer, S., Yang, Y., Schapka, E., Joshi, G., McQuade, T.J., Dharia, R.M., Dulchavsky, M., Ouyang, M., et al. (2016). Unbiased screen identifies aripiprazole as a modulator of abundance of the polyglutamine disease protein, ataxin-3. Brain J. Neurol. *139*, 2891–2908

Coutinho, P., Ruano, L., Loureiro, J.L., Cruz, V.T., Barros, J., Tuna, A., Barbot, C., Guimarães, J., Alonso, I., Silveira, I., et al. (2013). Hereditary Ataxia and Spastic Paraplegia in Portugal: A Population-Based Prevalence Study. JAMA Neurol. *70*, 746–755

Durr, A., Stevanin, G., Cancel, G., Duyckaerts, C., Abbas, N., Didierjean, O., Chneiweiss, H., Benomar, A., Lyon‐Caen, O., Julien, J., et al. (1996). Spinocerebellar ataxia 3 and machado-joseph disease: Clinical, molecular, and neuropathological features. Ann. Neurol. *39*, 490–499

Fahl, C.N., Branco, L.M.T., Bergo, F.P.G., D'Abreu, A., Lopes-Cendes, I., and França, M.C. (2015). Spinal Cord Damage in Machado-Joseph Disease. The Cerebellum *14*, 128–132

Guimarães, R.P., D'Abreu, A., Yasuda, C.L., França, M.C., Silva, B.H.B., Cappabianco, F.A.M., Bergo, F.P.G., Lopes-Cendes, I.T., and Cendes, F. (2013). A multimodal evaluation of microstructural white matter damage in spinocerebellar ataxia type 3. Mov. Disord. Off. J. Mov. Disord. Soc. *28*, 1125–1132

Harding, A.E. (1983). Classification of the hereditary ataxias and paraplegias. Lancet Lond. Engl. *1*, 1151–1155

Ilg, W., Synofzik, M., Brötz, D., Burkard, S., Giese, M.A., and Schöls, L. (2009). Intensive coordinative training improves motor performance in degenerative cerebellar disease. Neurology *73*, 1823–1830

Jacobi, H., Reetz, K., du Montcel, S.T., Bauer, P., Mariotti, C., Nanetti, L., Rakowicz, M., Sulek, A., Durr, A., Charles, P., et al. (2013). Biological and clinical characteristics of

individuals at risk for spinocerebellar ataxia types 1, 2, 3, and 6 in the longitudinal RISCA study: analysis of baseline data. Lancet Neurol. *12*, 650–658

Jacobi, H., du Montcel, S.T., Bauer, P., Giunti, P., Cook, A., Labrum, R., Parkinson, M.H., Durr, A., Brice, A., Charles, P., et al. (2015). Long-term disease progression in spinocerebellar ataxia types 1, 2, 3, and 6: a longitudinal cohort study. Lancet Neurol. *14*, 1101–1108

Jacobi, H., Montcel, S.T. du, Romanzetti, S., Harmuth, F., Mariotti, C., Nanetti, L., Rakowicz, M., Makowicz, G., Durr, A., Monin, M.-L., Filla, A., Roca, A., Schöls, L., Hengel, H., Infante, J., Kang, J.-S., Timmann, D., Casali, C., Masciullo, M., Baliko, L., Melegh, B., Nachbauer, W., Bürk-Gergs, K., Schulz, J.B., Riess, O., Reetz, K., Klockgether, T., (2020). Conversion of individuals at risk for spinocerebellar ataxia types 1, 2, 3, and 6 to manifest ataxia (RISCA): a longitudinal cohort study. The Lancet Neurology 19, 738–747

Joers, J.M., Deelchand, D.K., Lyu, T., Emir, U.E., Hutter, D., Gomez, C.M., Bushara, K.O., Eberly, L.E., and Öz, G. (2018). Neurochemical abnormalities in premanifest and early spinocerebellar ataxias. Ann. Neurol. *83*, 816–829

Klockgether, T. (1998). Autosomal dominant cerebellar ataxia type I. MRI-based volumetry of posterior fossa structures and basal ganglia in spinocerebellar ataxia types 1, 2 and 3. Brain *121*, 1687–1693

Klockgether, T. (2008). The clinical diagnosis of autosomal dominant spinocerebellar ataxias. The Cerebellum *7*, 101–105

Klockgether, T. (2010). Sporadic ataxia with adult onset: classification and diagnostic criteria. Lancet Neurol. *9*, 94–104

Lukas, C., Hahn, H.K., Bellenberg, B., Hellwig, K., Globas, C., Schimrigk, S.K., Köster, O., and Schöls, L. (2008). Spinal cord atrophy in spinocerebellar ataxia type 3 and 6: Impact on clinical disability. J. Neurol. *255*, 1244–1249

Martins, C.R., Martinez, A.R.M., de Rezende, T.J.R., Branco, L.M.T., Pedroso, J.L., Barsottini, O.G.P., Lopes-Cendes, I., and França, M.C. (2017). Spinal Cord Damage in Spinocerebellar Ataxia Type 1. The Cerebellum *16*, 792–796

Mattos, E.P. de, Leotti, V.B., Soong, B.-W., Raposo, M., Lima, M., Vasconcelos, J., Fussiger, H., Souza, G.N., Kersting, N., Furtado, G.V., et al. (2019). Age at onset prediction in spinocerebellar ataxia type 3 changes according to population of origin. Eur. J. Neurol. *26*, 113–120

de Mattos, E.P., Kolbe Musskopf, M., Leotti Torman, V., Saraiva-Pereira, M.L., and Jardim, L.B. (2018). Genetic risk factors for modulation of age at onset in Machado-Joseph disease/spinocerebellar ataxia type 3: a systematic review and meta-analysis. J. Neurol. Neurosurg. Psychiatry jnnp-2018-319200

Mendonça, N., França, M.C., Gonçalves, A.F., and Januário, C. (2018). Clinical Features of Machado-Joseph Disease. In Polyglutamine Disorders, C. Nóbrega, and L. Pereira de Almeida, eds. (Cham: Springer International Publishing), pp. 255–273

Moore, L.R., Rajpal, G., Dillingham, I.T., Qutob, M., Blumenstein, K.G., Gattis, D., Hung, G., Kordasiewicz, H.B., Paulson, H.L., and McLoughlin, H.S. (2017). Evaluation of Antisense Oligonucleotides Targeting ATXN3 in SCA3 Mouse Models. Mol. Ther. - Nucleic Acids *7*, 200–210

Paulson, H. (2012). Machado–Joseph disease/spinocerebellar ataxia type 3. In Handbook of Clinical Neurology, (Elsevier), pp. 437–449

Paulson, H. (2018). Chapter 9 - Repeat expansion diseases. In Handbook of Clinical Neurology, D.H. Geschwind, H.L. Paulson, and C. Klein, eds. (Elsevier), pp. 105–123

Paulson, H.L., Perez, M.K., Trottier, Y., Trojanowski, J.Q., Subramony, S.H., Das, S.S., Vig, P., Mandel, J.-L., Fischbeck, K.H., and Pittman, R.N. (1997). Intranuclear Inclusions of Expanded Polyglutamine Protein in Spinocerebellar Ataxia Type 3. Neuron *19*, 333–344

Paulson, H.L., Shakkottai, V.G., Clark, H.B., and Orr, H.T. (2017). Polyglutamine spinocerebellar ataxias — from genes to potential treatments. Nat. Rev. Neurosci. *18*, 613–626

Reetz, K., Costa, A.S., Mirzazade, S., Lehmann, A., Juzek, A., Rakowicz, M., Boguslawska, R., Schöls, L., Linnemann, C., Mariotti, C., et al. (2013). Genotype-specific patterns of atrophy progression are more sensitive than clinical decline in SCA1, SCA3 and SCA6. Brain *136*, 905–917

Rezende, T.J.R., de Paiva, J.L.R., Martinez, A.R.M., Lopes-Cendes, I., Pedroso, J.L., Barsottini, O.G.P., Cendes, F., and França, M.C. (2018). Structural signature of SCA3: From presymptomatic to late disease stages. Ann. Neurol

Ross, C.A., Aylward, E.H., Wild, E.J., Langbehn, D.R., Long, J.D., Warner, J.H., Scahill, R.I., Leavitt, B.R., Stout, J.C., Paulsen, J.S., et al. (2014). Huntington disease: natural history, biomarkers and prospects for therapeutics. Nat. Rev. Neurol. *10*, 204–216

Ruano, L., Melo, C., Silva, M.C., and Coutinho, P. (2014). The Global Epidemiology of Hereditary Ataxia and Spastic Paraplegia: A Systematic Review of Prevalence Studies. Neuroepidemiology *42*, 174–183

Rüb, U., Brunt, E.R., and Deller, T. (2008). New insights into the pathoanatomy of spinocerebellar ataxia type 3 (Machado–Joseph disease): Curr. Opin. Neurol. *21*, 111–116

Scherzed, W., Brunt, E.R., Heinsen, H., de Vos, R.A., Seidel, K., Bürk, K., Schöls, L., Auburger, G., Del Turco, D., Deller, T., et al. (2012). Pathoanatomy of Cerebellar Degeneration in Spinocerebellar Ataxia Type 2 (SCA2) and Type 3 (SCA3). The Cerebellum *11*, 749–760

Schmitz-Hübsch, T., du Montcel, S.T., Baliko, L., Berciano, J., Boesch, S., Depondt, C., Giunti, P., Globas, C., Infante, J., Kang, J.-S., et al. (2006). Scale for the assessment and rating of ataxia: development of a new clinical scale. Neurology *66*, 1717–1720

Schöls, L., Bauer, P., Schmidt, T., Schulte, T., and Riess, O. (2004). Autosomal dominant cerebellar ataxias: clinical features, genetics, and pathogenesis. Lancet Neurol. *3*, 291–304

Tabrizi, S.J., Leavitt, B.R., Landwehrmeyer, G.B., Wild, E.J., Saft, C., Barker, R.A., Blair, N.F., Craufurd, D., Priller, J., Rickards, H., Rosser, A., Kordasiewicz, H.B., Czech, C., Swayze, E.E., Norris, D.A., Baumann, T., Gerlach, I., Schobel, S.A., Paz, E., Smith, A.V., Bennett, C.F., Lane, R.M., (2019). Targeting Huntingtin Expression in Patients with Huntington's Disease. N. Engl. J. Med. 380, 2307–2316

Tezenas du Montcel, S., Durr, A., Rakowicz, M., Nanetti, L., Charles, P., Sulek, A., Mariotti, C., Rola, R., Schols, L., Bauer, P., et al. (2014). Prediction of the age at onset in spinocerebellar ataxia type 1, 2, 3 and 6. J. Med. Genet. *51*, 479–486

Warrenburg, B.P.C. van de, Hendriks, H., Dürr, A., Zuijlen, M.C.A. van, Stevanin, G., Camuzat, A., Sinke, R.J., Brice, A., and Kremer, B.P.H. (2005). Age at onset variance analysis in spinocerebellar ataxias: A study in a Dutch–French cohort. Ann. Neurol. *57*, 505–512

Wüllner, U., Klockgether, T., Petersen, D., Naegele, T., Dichgans, J., (1993). Magnetic resonance imaging in hereditary and idiopathic ataxia. Neurology 43, 318–318

Zu, T., Duvick, L.A., Kaytor, M.D., Berlinger, M.S., Zoghbi, H.Y., Clark, H.B., and Orr, H.T. (2004). Recovery from Polyglutamine-Induced Neurodegeneration in Conditional SCA1 Transgenic Mice. J. Neurosci. *24*, 8853–8861

Zu, T., Gibbens, B., Doty, N.S., Gomes-Pereira, M., Huguet, A., Stone, M.D., Margolis, J., Peterson, M., Markowski, T.W., Ingram, M.A.C., et al. (2011). Non-ATG–initiated translation directed by microsatellite expansions. Proc. Natl. Acad. Sci. *108*, 260–265

9. Acknowledgement

I wish to acknowledge the help provided by the German Center for Neurodegenerative Diseases (DZNE) and express my deep gratitude to my supervisors Thomas Klockgether and Jennifer Faber, for allowing me to experience such a well-organized scientific environment at the beginning of my professional life. I would like to extend my special thanks to my family for their unconditional support and Sevim & Necati Cengiz, for becoming my second family in Germany.

10. Publications

Faber J, Schaprian T, **Berkan K**, Reetz K, França MC Jr, de Rezende TJR, Hong J, Liao W, van de Warrenburg B, van Gaalen J, Durr A, Mochel F, Giunti P, Garcia-Moreno H, Schoels L, Hengel H, Synofzik M, Bender B, Oz G, Joers J, de Vries JJ, Kang JS, Timmann-Braun D, Jacobi H, Infante J, Joules R, Romanzetti S, Diedrichsen J, Schmid M, Wolz R, Klockgether T. Regional Brain and Spinal Cord Volume Loss in Spinocerebellar Ataxia Type 3. Mov Disord. 2021 Oct;36(10):2273-2281. doi: 10.1002/mds.28610. Epub 2021 May 5. PMID: 33951232. DOI: 10.1002/mds.28610

Kırbaş D., **Koyak B**. In the Footsteps of History of Neurology. The New History of Medicine Studies, 22:93110. 2016

Kırbaş D., **Koyak B**. Psychiatric Comorbidities in Neurological Diseases. Turkiye Klinikleri JNeurolSpecial Topics 2016;9(4):17. 2016

Kırbaş D., **Koyak B**. Armenian doctors during the first world war. The New History of Medicine Studies, 20:115-134. 2014 PMID: 30727699.